J. Phys. B: At. Mol. Opt. Phys. **40** (2007) S1–S44 doi:10.1088/0953-4075/40/9/S01

Weighted graph states and applications to spin chains, lattices and gases

L Hartmann[1], J Calsamiglia[2], W Dür[1,3] and H J Briegel[1,3]

[1] Institut für Theoretische Physik, Universität Innsbruck, Technikerstraße 25, A-6020 Innsbruck, Austria
[2] Grup de Física Teòrica and IFAE, Universitat Autònoma de Barcelona, Spain
[3] Institut für Quantenoptik und Quanteninformation der Österreichischen Akademie der Wissenschaften, Innsbruck, Austria

Received 21 November 2006, in final form 5 February 2007
Published 18 April 2007
Online at stacks.iop.org/JPhysB/40/S1

Abstract

Weighted graph states naturally arise when spin systems interact via an Ising-type interaction. First, we abstractly define the class of weighted graph states and demonstrate its computational accessibility. We show how reduced density matrices of a small number of spins ($\approx$10) can be computed from arbitrarily large systems using weighted graph techniques and projected entangled pair techniques, and we discuss various entanglement measures accessible from these reduced density matrices. Second, we apply these findings to spin chains and lattices with long-range interactions and analytically derive area laws for the scaling of block-wise entanglement. Then, we turn to disordered spin systems, spin gases, which are connected to random weighted graph states and which share their entanglement properties. Finally, we use a spin gas as a bath that introduces decoherence in single as well as multipartite spin systems. The microscopic, exact decoherence model we obtain can operate in different regimes and exhibit non-Markovian features as well as spatially correlated noise effects.

(Some figures in this article are in colour only in the electronic version)

1. Introduction

In quantum information science, entanglement and decoherence are prominent features. Entanglement has been identified as a key resource for quantum computation [1] and serves as a resource for various other tasks, including quantum key distribution, secret sharing and other distributed secure applications [2–4]. While entanglement in well-controllable systems is a desirable property, entanglement between a system and its (uncontrollable) environment leads to an unwanted effect known as decoherence. Decoherence is mostly seen as a threat to the quantum information one wishes to process. Thus, in all quantum information processing

tasks one wishes to have a system that has strong interactions among its components but an interaction with the external world as weak as possible, thereby minimizing the influence of decoherence. Hence there are two aspects of many-body quantum systems which have attracted considerable attention so far: (i) the properties, especially entanglement properties, of strongly interacting many-body systems, and (ii) the influence of decoherence processes on these systems.

In this paper, we will investigate these two key properties of many-body quantum systems. We will concentrate on a particular family of many-body systems, the so-called weighted graph states. This family is described by a polynomial number of parameters and includes states with a large variety of entanglement features, ranging from product states with no entanglement to states that are maximally entangled in several senses [5]. In particular, this family includes the 2D cluster states, which are known to be a universal resource for measurement-based quantum computation, and which have recently been shown to contain all possible kinds of entanglement [6]. More precisely, the maximum of any entanglement measure is obtained for 2D cluster states of sufficiently large size.

What makes the family of weighted graph states particularly appealing is the fact that interesting quantities can be *efficiently* evaluated. These quantities include two-point correlation functions, many entanglement measures, and the expectation values of all local observables, most prominently energy if the Hamiltonian is the sum of terms each having support on sufficiently few spins. This is in contrast to generic many-body states, which are usually described by exponentially many parameters, and where the evaluation of interesting quantities, e.g. reduced density operators, is not feasible. The latter problem strongly hinders our understanding of strongly correlated many-body quantum systems, because an analytic treatment as well as a classical simulation of such systems is a computationally hard problem. Only the treatment of relatively small systems, e.g. of a few tens of spin-1/2 particles, is possible. Weighted graph states, on the other hand, allow us to deal with thousands of spins, and enable a thorough investigation of the entanglement features. This makes weighted graph states an ideal test-bed for the investigation of strongly correlated many-body systems.

We will discuss such many-body quantum states from different perspectives, making full use of weighted graph states techniques. First, we study ordered lattice spin systems that interact pairwise via long-rang interactions. We investigate the entanglement properties of such states, e.g. localizable entanglement, block-wise entanglement and two-point correlation functions.

In a second part, we consider stochastic systems with random interactions, so-called spin gases. Here, the particles of a classical gas (e.g. a Boltzmann or lattice gas) are assumed to carry an additional spin quantum degree of freedom. The spins interact upon collision, and entanglement is generated—governed by the classical kinematics of the gas particles. We exhibit the relation between classical parameters describing the gas, e.g. temperature, and the entanglement features, such as the production rate of entanglement. Spin gases can be seen as a natural extension to the spin chain or lattice, where simply the order (fixed distances between the spins) has been given up. The transition from the ordered to the disordered case is very smooth since weighted graph states, on which the description is based, are independent of any geometry.

Third, such disordered systems also naturally lend themselves to be considered as a bath and to study decoherence when probe systems are immerged into them. When we expose a probe system to a spin gas, with which it becomes entangled, we can study the induced decoherence processes on the mircroscopic level. We obtain an exactly treatable model for a spin bath that shows non-Markovian behaviour. We can analyse this model to a large extent analytically and perform numerical simulations for spin gas environments of mesoscopic size

($\approx 10^5$ particles). This allows us to study effects of correlated versus uncorrelated noise, as well as Markovian versus non-Markovian decoherence processes, all of which show up in certain parameter regimes of such spin gases.

Although our investigations are based on the special class of weighted graph states, we nevertheless identify interesting features of strongly correlated many-body quantum states with respect to their entanglement and decoherence properties. Since decoherence is here just interpreted as an aspect of entanglement with an uncontrollable environment, a unified treatment of entanglement and decoherence is possible within our model and leads to interesting insights.

The present paper is based on three papers [7–9], where spin lattices with long-range interactions, spin gases and decoherence phenomena in spin gases were discussed. Since the weighted graph states and related methods are at the heart of these three papers, this paper makes weighted graph states and projected entangled pair states [10] a central topic and gives an overview about the techniques developed so far and about present and future applications [7–9, 11, 12]. Spin lattices and spin gases are described in more detail than in the former publications. Here, all analytical proofs are worked out. More discussion and supplementary material including plots are presented to highlight entanglement and decoherence effects.

The paper is organized as follows. Each section begins with a short introduction and a summary of the main results of that section. In section 2 we fix notation, discuss graph states and generalize to weighted graph states. The latter are at the heart of the description of both the spin lattices and the spin gases, and we show that reduced density matrices and other quantities—e.g. entanglement measures—can be computed efficiently for weighted graph states. Based on this knowledge, the entanglement properties of spin chains and lattices with long-range interactions are presented in section 3, while section 4 discusses these properties for semi-quantal lattice and Boltzmann gases. Decoherence in these spin systems is treated in section 5, and a summary follows in section 6.

2. Weighted graph states

After introducing some notation we define weighted graph states as a natural generalization of graph states. The weighted graph states form the core of all computations in this paper, and we show how to efficiently calculate reduced density matrices and other physical quantities such as entanglement measures. These results and the formalism behind them are central to the understanding of all later sections. In particular, we will show the following results:

- definition of weighted graph states;
- description in terms of interaction patterns and projected entangled pairs picture;
- efficient computation of reduced density matrices (from arbitrarily large states);
- extension to decoherence maps via Jamiolkowski isomorphism;
- discussion of computable quantities such as entanglement measures.

2.1. Notation

A graph is a set of vertices and edges. The latter describe which vertices are connected. Each graph can be represented by a diagram in a plane, where a vertex is represented by a point and the edges by lines joining two not necessarily distinct vertices. In this pictorial representation many concepts related to graphs can be visualized in a transparent manner. In the context of the present paper, vertices play the role of physical systems, whereas edges represent an interaction. Formally, an (undirected, finite) *graph* is a pair

$$G = (V, E)$$

of a finite set $V = \{1, \ldots, N\}$ and a set $E \subset [V]^2$, the elements of which are subsets of V with two elements each [13, 14]. The elements of V are called *vertices*, the elements of E *edges*. In the following, we will only consider *simple* graphs. A simple graph contains neither loops, i.e., edges connecting a vertex with itself, nor multiple edges, i.e., more than one edge between any given pair of vertices. Later we mainly regard a generalization of these simple graphs, where each edge $\{a, b\}$ is associated with a weight φ_{ab} representing the strength of the respective interaction.

In a d-dimensional lattice of arbitrary geometry we choose one lattice site as the origin $\mathbf{0} = (0, \ldots, 0)$ and label all the other sites by the lattice vectors $\boldsymbol{k} = (k_1, \ldots, k_d)$. If a site contains a spin, this spin inherits the label of the site. The distance between two spins $\boldsymbol{k}, \boldsymbol{l}$ is simply the Euclidean distance $r_{kl} = \|\boldsymbol{k} - \boldsymbol{l}\|$.

2.2. Weighted graph states

Weighted graph states are a generalization of graph states. The latter are a very important class of states in quantum information. They are e.g. at the heart of certain measurement-based models of a quantum computer (one-way quantum computer [15, 16]) and have been shown to contain a big class of error correcting codes, so-called Calderbank–Shor–Steane (CSS) codes [17, 18]. There are different ways to define graph states.

A first definition is based on the stabilizer formalism, a second on a representation over the binary field [5, 19, 20]. Since we will not use the techniques associated with these frameworks in this paper, we refer the interested reader to the review paper [5].

A third, equivalent definition is more physically motivated, and is the only one that can be generalized to weighted graph states. Consider a simple, undirected graph $G = (V, E)$, where the vertices V correspond to the physical particles. Every two vertices k, l that are connected by an edge correspond to two particles k, l that interact according to a non-local unitary $U_{kl} = \mathrm{e}^{-\mathrm{i}\varphi_{kl}H_{kl}}$, where φ_{kl} is a real number and H_{kl} a self-adjoint operator. The requirement that G is a simple, undirected graph poses restrictions on the unitaries U_{kl}, which must be commuting and symmetric under label swapping ($U_{kl} = U_{lk}$). Furthermore, graph states exclude weights on the edges, where a weight is just a real number, and one hence demands that the U_{kl} are the same for all k, l. For qubits, on which we will concentrate throughout the paper, commutativity already implies that the analysis can be restricted to interaction Hamiltonians that are up to local unitaries of Ising form $H_{kl}^I = \sigma_z^k \sigma_z^l$ [21]. To make this definition of graph states consistent with the first two, we demand that the interaction Hamiltonian is $H = \sum H_{kl} = \sum \frac{1}{4}\left(\mathbb{1} - \sigma_z^k\right) \otimes \left(\mathbb{1} - \sigma_z^l\right)$, where the sum runs over all edges. This Hamiltonian acts on the N-qubit initial state $|+\rangle^{\otimes N}$, where $|+\rangle = 2^{-1/2}(|0\rangle + |1\rangle)$ is the eigenstate of the Pauli operator σ_x with eigenvalue 1. The interaction phases are $\varphi_{kl} = \pi$ for all k, l, such that $U_{kl} = U_{kl}^\dagger$ is the controlled phase gate representable as the matrix $U_{kl} \cong \mathrm{diag}(1, 1, 1, -1)$. The graph states are now written as

$$|G\rangle = \prod_{\{a,b\} \in E} U_{ab} |+\rangle^{\otimes N}.$$

The definition via a physical interaction pattern can easily be generalized by dropping the demand that the underlying graph should not carry weights. Now, the set of edges E contains elements of the form $(\{k, l\}, \varphi_{kl})$ specifying the edges and the weights. We define again the commuting, unitary operators $U_{kl} = \mathrm{e}^{-\mathrm{i}\varphi_{kl}H_{kl}}$, which are again symmetric under label swapping, and we call the weights again interaction phases in this context, and the operators

H_{kl} interaction Hamiltonians. In the following, we will consider N spin-1/2 systems (qubits), which we label $1, \ldots, N$. We define

$$|G\rangle = \prod U_{kl}(\varphi_{kl})|+\rangle^{\otimes N},$$

where the product runs over all edges. The class of states we thereby obtain are the weighted graph states. As pointed out above, weighted graph states are no longer stabilizer states in general, so there is no generalization from graph states to weighted graph states in the stabilizer formalism.

We can write the information contained in the graph G into an $N \times N$ matrix Γ, where we set

$$\Gamma_{kl} = \varphi_{kl}$$

if $\{k, l\}$ is an edge in the graph, and $\Gamma_{kl} = 0$ otherwise. The matrix Γ is called the adjacency matrix, and it is symmetric with zero diagonal by the requirement that it represents a simple, undirected graph.

To make the connection to physics stronger, we take the total Hamiltonian to be

$$H(t) = \sum_{k<l} g_{kl}(t) H_{kl}, \tag{1}$$

where the functions $g_{kl}(t)$ are determined by the particular two-body interactions between qubits $k, l \in \{1, \ldots, N\}$. The functions g_{kl} may also be constant or depend implicitly on time, i.e., they may e.g. depend on the position of spin particles, which, in their turn, depend on time. A weighted graph state is created by the time evolution of the initial product state $|+\rangle^{\otimes N}$ such that, after a time t, we have

$$|\Psi_t\rangle = U_t|+\rangle^{\otimes N} = \prod_{k>l} U_{kl}(\varphi_{kl}(t))|+\rangle^{\otimes N}, \tag{2}$$

where again $U_{kl}(\varphi_{kl}(t)) = \mathrm{e}^{-\mathrm{i}\varphi_{kl}(t)H_{kl}}$ and

$$\varphi_{kl}(t) = \int_0^t g_{kl}(t')\,\mathrm{d}t'. \tag{3}$$

At a time t, the quantum state is fully determined by the $N(N-1)/2$ phases $\varphi_{kl}(t)$, which in turn are determined by the interaction history of the N particles.

To ensure that the set of weighted graph states contain the graph states, we will, unless explicitly stated otherwise, throughout the paper set $H_{kl} = \frac{1}{4}\left(\mathbb{1} - \sigma_z^k\right) \otimes \left(\mathbb{1} - \sigma_z^l\right) = |11\rangle_{kl}\langle 11|$. Then, the unitaries are controlled-phase gates $U_{kl}(\varphi_{kl}) \equiv \mathrm{diag}(1, 1, 1, \mathrm{e}^{\mathrm{i}\varphi_{kl}})$. Note that the choice of $|+\rangle^{\otimes N}$ as initial state is not essential. All product input states could be chosen and some more general states as discussed in section 2.5.

The evolution of the initial state $|+\rangle^{\otimes N}$ can be straightforwardly described in the standard basis $\{|0\rangle, |1\rangle\}^{\otimes N}$ with the help of the adjacency matrix $\Gamma(t)$ as

$$U_t|+\rangle^{\otimes N} = 2^{-\frac{N}{2}} \sum_s U_t|s\rangle = 2^{-\frac{N}{2}} \sum_s \mathrm{e}^{\mathrm{i}\frac{1}{2}s\cdot\Gamma(t)\cdot s}|s\rangle, \tag{4}$$

where the sum is carried out over all N-digit binary vectors s, i.e., over all 2^N different combinations of zeros and ones. Moreover, although the description in (4) requires an exponential number of terms, we will see that the reduced density matrices and other quantities can in fact be computed efficiently using the adjacency matrix alone.

There is another way to describe weighted graph states. Verstraete and Cirac proposed a description of graph states in terms of valence bond solids (VBS) [22]. There, certain maximally entangled pairs of states are being projected into lower dimensional Hilbert spaces

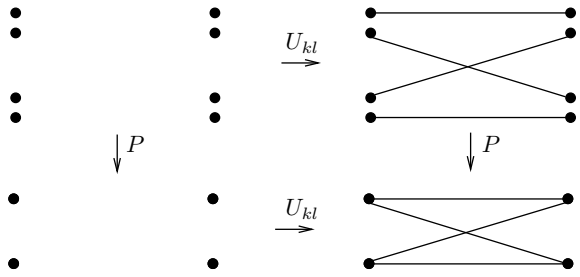

Figure 1. Schematic commuting diagram showing the equivalence of the PEPs and standard picture for describing weighted graph states.

to form graph states. Instead of maximally entangled pairs of qubits, we use pairs where the degree of entanglement depends on φ_{kl}. In previous publications, [7, 8], we called this a generalized VBS-picture, but in the meantime the term 'projected entangled pairs' (PEPs) [10] has become more widely known. Our approach is a generalized PEPs picture, but we will omit 'generalized' and simply use 'PEPs' from now on. With PEPs-methods we now develop a description of weighted graph states.

Consider a weighted graph state defined on N qubits. Each of the N physical qubits is replaced by $N-1$ (virtual) qubits. For instance, qubit k is replaced by $N-1$ virtual qubits $k_1, k_2, \ldots, \hat{k}_k, \ldots, k_N$ where the labelling is chosen such that k_k is missing. The PEPs state $|\tilde{\Psi}_t\rangle$ is a state of the $N(N-1)$ virtual qubits defined on the corresponding Hilbert space $\mathcal{H} = [(\mathbb{C}^2)^{N-1}]^N$. The state $|\tilde{\Psi}_t\rangle$ consists of $N(N-1)/2$ independent, non-maximally entangled pairs $|\varphi_{k_l k_k}\rangle$, where there is always one pair corresponding to two parties. For instance, the pair $|\varphi_{k_l k_k}\rangle = U_{k,l}|+\rangle_{k_l}|+\rangle_{l_k}$ corresponds to parties k, l and involves the virtual qubits k_l of party k and l_k of party l. The total state $|\tilde{\Psi}_t\rangle$ is given by a tensor product of all pairs, $|\tilde{\Psi}_t\rangle = \otimes_{k<l}|\varphi_{k_l k_k}\rangle$. Up to a normalization factor, we obtain the corresponding weighted graph state $|\Psi_t\rangle = U|+\rangle^{\otimes N}$ from $|\tilde{\Psi}_t\rangle$ by performing local projections $P_k = |0_k\rangle\langle \mathbf{0_k}| + |1_k\rangle\langle \mathbf{1_k}|$ onto two-dimensional subspaces at all locations k, where $\mathbf{k} = (k_1, \ldots \hat{k}_k, k_N)$ and $|\mathbf{0}\rangle = |00\ldots0\rangle$, $|\mathbf{1}\rangle = |11\ldots1\rangle$. The PEPs state $|\tilde{\Psi}_t\rangle$, together with the projection $\otimes_k P_k$, thus provides an equivalent description of the state $|\Psi_t\rangle$. To sum up, we have seen that the (symbolic) diagram in figure 1 commutes.

We have established two descriptions of weighted graph states, the straightforward generalization of the interaction pattern that creates graph states and the PEPs picture. In the following, we use the both the standard and PEPS description to determine reduced density operators ρ_A before we describe entanglement measures and other computable quantities.

2.3. Reduced density matrices

We begin by deriving reduced density matrices in the PEPs picture, then show that we obtain the same result by directly computing the reduced density matrix from the weighted graph state. We also derive an expression solely in terms of the adjacency matrix and finally give a completely positive map taking the initial state $\rho = (|+\rangle\langle+|)^{\otimes N}$ to the reduced density matrix of a weighted graph state.

2.3.1. Reduced density matrices via PEPs picture. We denote by A an arbitrary subset of the N qubits, and we call the set of remaining qubits B. Because all U_{kl} commute and because

unitaries between all pairs of qubits in the set B do not influence $\rho_A = \mathrm{tr}_B(|\Psi_t\rangle\langle\Psi_t|)$, we can write

$$\rho_A = \prod_{k,l\in A} U_{kl}\mathrm{tr}_B|\Psi_t'\rangle\langle\Psi_t'|U_{kl}^\dagger, \tag{5}$$

with $|\Psi_t'\rangle = \prod_{k\in A,l\in B} U_{kl}|+\rangle^{\otimes N}$. We now determine $\rho_A' = \mathrm{tr}_B|\Psi_t'\rangle\langle\Psi_t'|$ in the PEPs-picture, i.e., we start with the state

$$|\tilde{\Psi}_t'\rangle = \bigotimes_{k\in A,l\in B} U_{kl}|+\rangle_{k_i}|+\rangle_{l_j}. \tag{6}$$

For the following argumentation it is crucial that $U_{kl} = \mathbb{1}$ for $k, l \in B$ as is the case for $|\tilde{\Psi}_t'\rangle$ but not for $|\tilde{\Psi}_t\rangle$. Performing the projections P_l on all particles $l \in B$ (but not in A) leaves us with a state of the form $\otimes_{l\in B}[\prod_{k\in A} U_{kl}|+\rangle_{\mathbf{k}}|+\rangle_l]$. We have a tensor product of $|B|$ states, where in the lth state particle $l \in B$ is entangled with a virtual system A. For each of these states we can independently calculate the reduced density operator with respect to A. We simply trace out particle l and obtain

$$\rho_A'(l) = \tfrac{1}{2}(|+\rangle_A\langle+| + |\varphi_l\rangle_A\langle\varphi_l|), \tag{7}$$

with $|\varphi_l\rangle_A = \otimes_{k\in A}(|0\rangle + \mathrm{e}^{\mathrm{i}\varphi_{kl}}|1\rangle)/\sqrt{2}$. Now, we perform the projections P_k for all $k \in A$. The resulting density operator ρ_A' is (up to normalization) given by the *Hadamard product* of all density operators $\rho_A'(l)$, where the Hadamard product of two matrices corresponds to component-wise multiplication in the computational basis. We prove this statement for general density operators $\rho_A(i) = \sum(\alpha_i)_{m_i n_i}|m_i\rangle\langle n_i|$, where i runs over some index set. The equation reads $P(\otimes_i \rho_A(i))P^\dagger = \otimes_j(|0\rangle_{j\mathbf{j}}\langle\mathbf{0}| + |1\rangle_{j\mathbf{j}}\langle\mathbf{1}|)(\otimes_i\big(\sum_{m_i n_i}(\alpha_i)_{m_i n_i}|m_i\rangle\langle n_i|\big) \otimes_j (|\mathbf{0}\rangle_{\mathbf{j}j}\langle 0| + |\mathbf{1}\rangle_{\mathbf{j}j}\langle 1|)$. Here, $\mathbf{j}$, $|\mathbf{0}\rangle$ and $|\mathbf{1}\rangle$ have as many components as the index set over which i runs. The projectors P_j, acting on the jth components of all the basis states $|m_i\rangle$, collapse the sums because they are nonzero only when the components are equal. Hence, the equation becomes $P(\otimes_i \rho_A(i))P^\dagger = \sum_{m,n}\big(\prod_i(\alpha_i)_{mn}\big)|m\rangle\langle n|$, and we see that the matrix representations of the density operators $\rho_A(i)$ are Hadamard-multiplied in the computational basis as claimed.

The reduced density matrix ρ_A' is a $2^{|A|} \times 2^{|A|}$ matrix. When we label the matrix entries by binary vectors $\mathbf{m}$ of length $|A|$, with components m_k, $k \in A$, the $\mathbf{m}$, $\mathbf{n}$th matrix entry is

$$\langle\mathbf{m}|\prod_{l\in B}(|+\rangle_A\langle+| + |\phi_l\rangle_A\langle\phi_l|)|\mathbf{n}\rangle = \prod_{l\in B}\left(1 + \exp\left\{\mathrm{i}\sum_{k\in A}\left(\varphi_{kl}^{n_k} - \varphi_{kl}^{m_k}\right)\right\}\right).$$

Finally, we obtain the reduced density operator ρ_A from ρ_A' by taking into account interactions within A leading to

$$\rho_A = \prod_{k,l\in A} U_{kl}\rho_A' U_{kl}^\dagger.$$

As a last step, we must normalize the resulting state.

2.3.2. Reduced density matrices directly computed from the weighted graph states. Now, we compute the reduced density matrix directly from the weighted graph state. Disregarding interactions within partition A and also within B, we start again with the state

$$|\Psi_t'\rangle = \prod_{k\in A,l\in B} U_{kl}|+\rangle^{\otimes|A|}|+\rangle^{\otimes|B|} = \sum_{\mathbf{m}}|\mathbf{m}\rangle_A \bigotimes_{l\in B}\left|\sum_{k\in A}\varphi_{kl}^{m_k}\right\rangle_l.$$

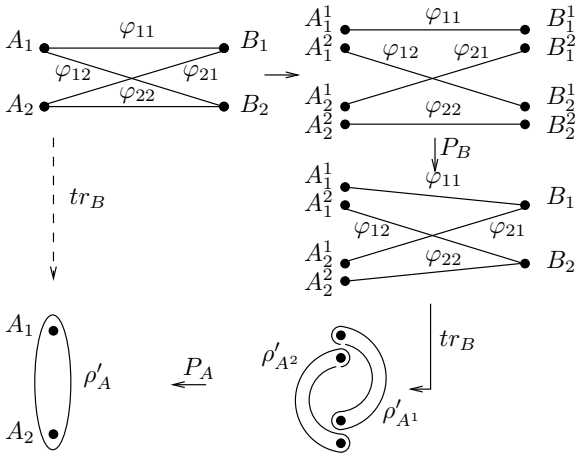

Figure 2. Schematic commuting diagram showing the computation of a reduced density matrix by directly tracing out the subsystem B (dashed arrow) or by invoking the PEPs picture (solid arrows).

Here we put again $|\varphi\rangle = 2^{-1/2}(|0\rangle + \mathrm{e}^{\mathrm{i}\varphi}|1\rangle)$, and $\mathbf{m}$ is a binary vector as above. The $\mathbf{m}, \mathbf{n}$th matrix entry of $\mathrm{tr_B}|\Psi'_\mathrm{t}\rangle\langle\Psi'_\mathrm{t}|$ is

$$\prod_{l\in B}\left\langle \sum_{k\in A}\varphi_{kl}^{m_k}\middle|\sum_{k\in A}\varphi_{kl}^{n_k}\right\rangle = 2^{-|B|}\prod_{l\in B}\left(1+\exp\left\{\mathrm{i}\sum_{k\in A}\left(\varphi_{kl}^{n_k}-\varphi_{kl}^{m_k}\right)\right\}\right),$$

since $\langle\psi|\varphi\rangle = 2^{-1}(1 + \exp\{\mathrm{i}(\varphi - \psi)\})$. Later we will use $2^{-1}(1 + \exp\{\mathrm{i}\varphi\}) = \cos(\varphi/2)\exp\{\mathrm{i}\varphi/2\}$ to write such expressions in a modulus-phase notation. We obtained the same matrix element as above apart from a normalization factor, since, in the PEPs picture, we normalize only at the end of the computation. Again, the interactions within partition A must now be taken into account to obtain ρ_A from ρ'_A.

To summarize, we have seen that the (schematic) diagram in figure 2 does, indeed, commute.

The PEPs picture and the direct approach are equivalent. The direct approach has the advantage that it is conceptually straightforward and normalization is conserved at all times. The PEPs ansatz, on the other hand, shows more clearly how the reduced density matrix is built up from the qubits in the remaining partition B. We can use the properties of the Hadamard product to derive properties of other quantities when qubits are added to the partition B. We will come back to this when we discuss the entropy of entanglement between partitions A and B. Also, the PEPs ansatz has the merit that we can deal with one qubit in B at a time, eliminating the need to know all the interaction phases φ_{kl} in advance. This is important to save memory space when computing large systems.

2.3.3. Reduced density matrices from the adjacency matrix. Let us re-express the computation of reduced density matrices with the help of the adjacency matrix Γ. Since the unitary operations in (2) commute with each other, the evolution of a set A of N_A particles can be separated into two contributions. The first entangles particles within A and is determined by the block Γ_{AA} of the adjacency matrix. The second contribution couples the subsystem A to the rest B of the system through the off-diagonal block Γ_{AB}. The effect of the latter can be obtained by tracing out the set of particles B from the state $|\Psi_t\rangle$:

$$\rho'_A = \frac{1}{2^N}\mathrm{tr}_B \sum_{s,s'}^{2^N-1} \mathrm{e}^{\mathrm{i}\frac{1}{2}(\boldsymbol{s}.\Gamma.\boldsymbol{s}-\boldsymbol{s}'\cdot\Gamma\cdot\boldsymbol{s}')}|\boldsymbol{s}\rangle\langle\boldsymbol{s}'|$$
$$= \frac{1}{2^{N_A}} \sum_{s_A,s'_A} \left(\frac{1}{2^{N_B}} \sum_{s_B} \mathrm{e}^{\mathrm{i}(\boldsymbol{s}_A-\boldsymbol{s}'_A)\cdot\Gamma_{AB}\cdot\boldsymbol{s}_B} \right) |\boldsymbol{s}_A\rangle\langle\boldsymbol{s}'_A|. \tag{8}$$

The second equality is obtained by writing $|s\rangle = |s_A\rangle|s_B\rangle$, and the prime in ρ'_A indicates that interactions within subsystem A are not taken into account (Γ_{AA} is set to zero). Clearly, the values of the block Γ_{BB} do not affect the properties of either ρ_A or ρ'_A. In the standard basis, each off-diagonal element—or 'coherence'—of the initial state is decreased by a factor, $\rho'_{s_A s'_A}(t) = C_{s_A s'_A}\rho'_{s_A s'_A}(0)$, while diagonal elements remain untouched. The multiplying factor can be conveniently written as

$$C_{s_A s'_A} = \mathrm{e}^{\mathrm{i}\frac{1}{2}\sum_k(\boldsymbol{s}_A-\boldsymbol{s}'_A)\cdot\boldsymbol{\Gamma}_k} \prod_{k=1}^{N_B} \cos\left[\tfrac{1}{2}(\boldsymbol{s}_A - \boldsymbol{s}'_A)\cdot\boldsymbol{\Gamma}_k\right], \tag{9}$$

where we have defined the N_A-dimensional vector $(\boldsymbol{\Gamma}_k)_j = \Gamma_{kj}$ for each particle $k \in B$. In this form, we see that the total effect of the interactions with particles in B on a particular coherence $C_{s_A s'_A}$ of ρ_A can be obtained by multiplying the effects of each individual particle in B. More succinctly, if $\rho_A(k)$ is the state of the subsystem due to the sole effect of particle $k \in B$, then the state ρ_A is obtained (up to normalization) by the *Hadamard product* of all $\{\rho_A(k)\}_{k=1}^{N_B}$ written in the standard basis, that is by their component-wise multiplication. This observation can also be understood within the context of the PEPs picture as explained above [7]. The decomposition into Hadamard products allows one to read off the matrix elements of ρ_A from the adjacency matrix.

2.3.4. Evolution map for the reduced density matrix. There is another way to look at (9) that we will later adopt to study decoherence phenomena. This equation is effectively a map that sends any initial state $\rho(0)$ of some system A to its state at time t: $\mathcal{E}_t[\rho(0)] = \rho(t)$. Here it is not required that both system A and environment B be jointly in a weighted graph state (they are, however, automatically in a generalized version thereof; see subsection 2.5). The only requirements are that the system interact with the environment by the Hamiltonian (1) and that the interactions within the environment B fulfil conditions specified later in section 5. We can conveniently characterize this map by its action on the computational operator-basis: $\mathcal{E}_t(|s\rangle\langle s'|) = C_{ss'}|s\rangle\langle s'|$, where $C_{ss'}$ is given in (9). Alternatively, if we write C for the matrix consisting of the entries from (9), and use the symbol $\circ$ for the Hadamard product, then the map above is of the form $\mathcal{E}_t[\rho(0)] = \rho(t) = C \circ \rho(0)$.This means that the Hadamard product structure is inherited from states to maps: in particular the map $\mathcal{E}_t$ induced by all particles in B can be obtained by applying successively the maps $\mathcal{E}_t^{(l)}$ corresponding to each individual particle l in B, $\mathcal{E}_t = \mathcal{E}_t^{(1)} \ldots \mathcal{E}_t^{(N_B)}$.

One can write this transformation in the Pauli basis ($\sigma_0 \equiv \mathbb{1}$, $\sigma_1 \equiv \sigma_x$, $\sigma_2 \equiv \sigma_y$, $\sigma_3 \equiv \sigma_z$, and tensor products thereof) by making use of the Jamiolkowski isomorphism. This isomorphism between completely positive maps and higher-dimensional mixed states [23] allows one to write the Pauli representation of the map in a quite straightforward manner. In particular, a map $\mathcal{E}_t$ can be equivalently described by the state $E_t = \mathbb{1}^{A'} \otimes \mathcal{E}_t^A|\Phi\rangle\langle\Phi|$. Here, $|\Phi\rangle = \otimes_{k=1}^{|A|}|\varphi^+\rangle_{k'k}$, $|\varphi^+\rangle \propto |00\rangle + |11\rangle$, and A' is an auxiliary system with the same dimension as A. That is, specifying a map is equivalent to specifying the state that results from applying the map to a part of a maximally entangled bi-partite system.

Moreover, in the Pauli basis, the coefficients of the map are given by the coefficients of the state E_t written in (tensor products of) Bell bases, i.e., $\mathcal{E}_t\rho =$

$\sum \lambda_{k_1\ldots k_{N_A},l_1\ldots l_{N_A}} \sigma_{k_1}\ldots\sigma_{k_{N_A}}\rho\sigma_{l_1}\ldots\sigma_{l_{N_A}}$, where $\lambda_{k_1\ldots k_{N_A},l_1\ldots l_{N_A}} = \langle\varphi_{k_1\ldots k_{N_A}}|E_t|\varphi_{l_1\ldots l_{N_A}}\rangle$ with $|\varphi_{k_1\ldots k_{N_A}}\rangle = \mathbb{1}_{A'}\otimes(\sigma_{k_1}\ldots\sigma_{k_{N_A}})_A|\Phi\rangle$. We can separately consider maps (or equivalently the states $E_t^{(l)}$) resulting from the interaction of the system with a single particle l in the environment. We find $E_t^{(l)} = 1/2\big(|\Phi\rangle\langle\Phi| + \otimes_{k=1}^{|A|}|\chi_k\rangle\langle\chi_k|\big)$ with $|\chi_k\rangle_{k'k} = 1/\sqrt{2}(|00\rangle + \mathrm{e}^{\mathrm{i}\varphi_{kl}(t)}|11\rangle)$, where $\varphi_{kl}(t)$ is the effective interaction phase between particles $k\in A$ and $l\in B$. The state E_t describing the total decoherence process incorporates the influence of all particles $l\in B$. We obtain E_t (up to a normalization factor $2^{(N_A-1)N_B}$) by calculating the Hadamard product of states $E_t^{(l)}$ written in the standard basis, i.e., by component-wise multiplication. The matrix elements of E_t expressed in the tensor Bell basis finally determine $\mathcal{E}_t$. We find that E_t has nonzero components only in the subspace spanned by $\{|\varphi_{k_1\ldots k_{N_A}}\rangle\}$ with $k_j\in\{0,3\}$. The map $\mathcal{E}$ thus contains only tensor products of Pauli operators $\mathbb{1}$ and σ_z. To illustrate this method, we will compute the Pauli representation of the map for one qubit in section 5.

It is a matter of taste whether one prefers to work in the PEPs picture, to directly compute reduced density matrices from the weighted graph states or to use the adjacency matrix or completely positive maps for this purpose. All variants are equivalent, but reflect a slightly different way of thinking about the weighted graph states. We will later switch between these variants depending on the physical context.

The important message, however, is that the methods outlined above provide an efficient way to calculate reduced density operators. The computation time is linear in the number $|B|$ of particles in the remaining system (but exponential in $|A|$), as opposed to an exponential scaling in $N = |A| + |B|$ of computation time and memory cost for general pure states (because the partial trace has to be performed over all 2^{N_B} basis states in B). Hence, for arbitrary large systems, all quantities that depend on the reduced density operator of a small number of qubits can be calculated efficiently. We discuss such quantities in the following.

2.4. Entanglement measures and other computable quantities

Whereas entanglement of bipartite systems is rather well understood, entanglement properties of multipartite systems, such as the weighted graph states, are in general difficult to determine. However, for pure global states, we can already get a broad picture of the entanglement in a multipartite system by considering all possible 2^{N-1} splits of the set of particles into two groups (A and B). The entanglement properties with respect to such bipartitions $A-B$ are completely determined by the eigenvalues of the reduced density operator $\rho_A = \mathrm{tr}_B|\Psi_t\rangle\langle\Psi_t|$, and one can use the entropy of entanglement

$$S_{\boldsymbol{A}} = -\mathrm{tr}(\rho_A\log_2\rho_A) \tag{10}$$

to quantify them. We pointed out already that the calculation of reduced density matrices is, in general, very difficult if not impossible (exponential scaling in both N_A and N_B). Even to ascertain whether a given system is entangled or not ($\mathrm{rank}(\rho_A) > 1$ or $= 1$) may be impossible. For weighted graph states $|\Psi_t\rangle$ we can use (9) to determine in an efficient way the density matrix ρ_A of small subsystems A (up to $|A| < 10$) and hence calculate the entropy of entanglement with respect to all such bipartitions. Clearly, $0\leqslant S_{\boldsymbol{A}}\leqslant|A|$, where $S_{\boldsymbol{A}} = |A|$ indicates maximal entanglement between the partitions A and B. For partitions with more than ten qubits, we make use of the strong subadditivity of the entropy to derive upper bounds on $S_{\boldsymbol{A}}$. By breaking a partition of size $|A|$ into n sub-partitions A_i of size $|A_i| = |A|/n$, we obtain

$$S_{\boldsymbol{A}} = S(\rho_A)\leqslant\sum_{i=1}^{n-1}S\big(\rho_{A_i,A_{i+1}}\big) - \sum_{i=2}^{n-1}\mathcal{S}\big(\rho_{A_i}\big), \tag{11}$$

where $\rho_{A_i,A_{i+1}}$ is the reduced density matrix of a sub-partition $A_i\cup A_{i+1}$ of size $2|A|/n$.

The unitary operations U_{kl} with $k, l \in A$ do not change the entropy $S(\rho_A)$ and hence the reduced density operator ρ'_A can be used directly since $S(\rho_A) = S(\rho'_A)$. Nevertheless, upper bounds on the entropy are different for ρ_A and ρ'_A, where the latter turn out to be more stringent and will hence be used in the following.

The fact that the total reduced density operator is given by the Hadamard product of reduced density operators with respect to all particles in the system B can be exploited to prove monotonicity properties of $S(\rho'_A)$. For a fixed size $|A|$, we add one particle j to B. The reduced density operator is updated by Hadamard multiplication with $\rho'_A(j)$. From theorem 5.5.12 in [24] follows that the eigenvalues of the resulting density operator are majorized by the eigenvalues of the initial one, which implies that the entropy increases [25]. As a consequence we obtain lower bounds on the entropy of entanglement $S(\rho'_A)$ when we take into account only a subset $\tilde{B} \subset B$ of all particles (and ignore the other particles in B).

We can also compute quantities such as the multipartite Meyer–Wallach pure-state entanglement measure $E_{\mathrm{MW}} = 2\big[1 - 1/N \sum_k \mathrm{tr}\big(\rho_k^2\big)\big]$ [26, 27], which only depends on single-body density matrices. The same is true for 'correlation strengths' [28] of finite blocks, which follow from the reduced density matrices of the block and all of its reductions.

Furthermore, we have a simple criterion for the presence of entanglement [8]: the state $|\Psi_t\rangle$ is entangled with respect to the partition $A-B$ iff the two groups are connected (i.e., an interaction between some particle in A and some particle in B has taken place with an interaction phase that is not an integer multiple of 2π).

A different aspect of (global) multipartite entanglement is the question whether entanglement can be created (localized) between two arbitrary subsets of particles $A_1 - A_2$ by performing *local* operations on the other particles. For weighted graph states we find that this is the case iff there exists a path between A_1 and A_2 in the corresponding graph. The necessity of the condition is obvious, while the sufficiency follows from these two facts: (i) collisions where particle k is involved can be erased (up to local operations) by measuring k in the z-basis $\{|0\rangle, |1\rangle\}$. (ii) If some particle i is connected to a particle j via an intermediate particle k with generic phases φ_{ik} and φ_{kj}, then a projection onto an arbitrary state $|u\rangle_k \notin \{|0\rangle, |1\rangle\}$ effectively creates an entangling operation on the particles i and j (unless both are in one of the states of the standard basis). One can hence perform measurements (e.g. along the x-axis) on the particles found in the connecting path, z-measurements on the rest, and ends up with an entangled pair. Determining whether two particles in a graph are connected is known as the reachability problem, which can be solved by an algorithm with run time of $O(N^2)$.

One can try to optimize over all local measurement strategies to obtain the maximum average entanglement, the so-called *localizable entanglement* [29]. The localizable entanglement is bounded from below and above, $Q^{k,l}_{\max} \leqslant E^{k,l}_L \leqslant E^{k,l}_A$, where $E^{k,l}_A$ is the concurrence of assistance [30], and $Q^{k,l}_{\max}$ is the maximal classical correlation between two particles. The maximal classical correlation is given by the largest singular value of the matrix $Q^{k,l}_{\alpha,\beta}$ [29], where

$$Q^{k,l}_{\alpha,\beta} = \big\langle \sigma^{(k)}_\alpha \sigma^{(l)}_\beta \big\rangle - \big\langle \sigma^{(k)}_\alpha \big\rangle \big\langle \sigma^{(l)}_\beta \big\rangle \tag{12}$$

are two-point correlation functions and $\alpha, \beta \in \{1, 2, 3\}$. Higher order correlation functions can be computed like those used in generalized n-party Bell-inequalities [31, 32]. Note that the localizable entanglement naturally leads to a definition of entanglement length as the typical length scale at which the localizable entanglement decays [29]. Formally expressed, we have $\xi_E^{-1} = \lim_{\|k-l\|\to\infty} \big(\ln E^{k,l}_L \big/ \|k-l\| \big)$, where $\|k-l\|$ is the distance between the spins k and l. The classical correlation length is a lower bound to the entanglement length, hence a diverging correlation length implies a diverging entanglement length.

Before closing this subsection on entanglement measures, we want to make a point concerning the choice of Hamiltonian. We have seen in several ways that the matrix elements of the state of a sub-system are multiplied by a complex factor in the computational basis due to interactions with particles of the remaining part of the system [see e.g. (9)]. When calculating locally invariant quantities such as the above entanglement measures we can simplify calculations by neglecting the phase factor in (9) because it can be cancelled by acting with the following local unitary on the sub-system:

$$U_{\text{local}}|s_A\rangle = \prod_{a=1}^{N_A} \mathrm{e}^{-\mathrm{i}(\sum_k \Gamma_{ak})|1\rangle_a\langle 1|}|s_A\rangle = \mathrm{e}^{-\mathrm{i}\frac{1}{2}\sum_k \boldsymbol{s}_A\cdot\boldsymbol{\Gamma}_k}|s_A\rangle. \tag{13}$$

2.5. Generalizations of weighted graph states

As a first generalization of weighted graph states, we can use any initial product state $|\Psi_0\rangle = \otimes_{n=1}^{N}|\chi_n\rangle$ where $|\chi_n\rangle = \alpha_n|0\rangle + \beta_n|1\rangle$ instead of the special product state state $|+\rangle^{\otimes N}$. Again, we compute the matrix entries of $\rho'_A = \mathrm{tr}_{\mathrm{B}}|\Psi'_{\mathrm{t}}\rangle\langle\Psi'_{\mathrm{t}}|$. Using A-binary vectors $\mathbf{m}$ with coefficients m_k and binarily complementary coefficients $\overline{m}_k := \mathrm{not}(\mathrm{m_k})$, the $\mathbf{m}, \mathbf{n}$th matrix entry is

$$\left(\prod_{k\in A}\alpha_k^{\overline{m}_k}(\alpha_k^*)^{\overline{n}_k}\beta_k^{m_k}(\beta_k^*)^{n_k}\right)\prod_{l\in B}\left(|\alpha_l|^2 + |\beta_l|^2\exp\left\{\mathrm{i}\sum_{k\in A}(\varphi_{kl}m_k - \varphi_{kl}n_k)\right\}\right),$$

where we use the convention $0^0 := 1$.

The same can also be expressed in the PEPs picture. In this case, the (unnormalized) PEPs-like state is of the form $|\tilde{\Psi}_t\rangle = \otimes_{k,l}|\varphi_{k_i l_j}\rangle$ with $|\varphi_{k_i l_j}\rangle = U_{kl}|\sqrt[N-1]{\chi_k}\rangle_{k_i}|\sqrt[N-1]{\chi_l}\rangle_{l_j}$, where $|\chi\rangle = \alpha|0\rangle + \beta|1\rangle$ and $|\sqrt[n]{\chi}\rangle \equiv \sqrt[n]{\alpha}|0\rangle + \sqrt[n]{\beta}|1\rangle$. Apart from this subsection, we will not consider more general initial states in the rest of the paper and hence do not elaborate on this point.

A second generalization is easily obtained from the first. If we superpose only $\chi = \mathrm{poly}(N)$, i.e., polynomially many product states, the resulting state $|\Psi_0\rangle = \sum_{j=1}^{\chi}|\alpha_1^j\alpha_2^j\cdots\alpha_N^j\rangle$ can be taken as an initial state. Still, reduced density matrices can be computed efficiently if this state evolves under the Hamiltonian (1) since this was true for all χ summands individually. For an arbitrary state $\chi \neq \mathrm{poly}(N)$ in any product basis, so the above generalization can equivalently be rephrased in the following way. There is an efficient description as long as the Schmidt measure [33] of the initial state is small (polynomially many Schmidt coefficients).

Since we can compute reduced density matrices of small subsystems we can, at the same time, compute the expectation values of any observable that is the sum of terms with support on only a few qubits. For many models, these observables include the energy, and hence one can use the class of weighted graph states as a variational class to find ground-state approximations for other strongly interacting spin systems. The advantage of weighted graph states compared to DMRG lies in their independence of any geometry and spatial dimensionality and, as we will later show, in their entanglement properties: weighted graph states may contain an arbitrary amount of entanglement as opposed to the matrix product states used in DMRG. In [11] states of N qubits, which are slightly more general than the weighted graph states defined here, were used for ground-state approximations. Specifically, with a filtering operation $D_a = \mathrm{diag}(1, d_a)$, $d_a \in \mathbb{C}$, and a general 1-qubit unitary operation U_a, states of the form

$$|\Psi_{\Gamma,\boldsymbol{d},U}\rangle \propto \prod_{a=1}^{N} U_a D_a \prod_{b=a+1}^{N} U_{ab}(\varphi_{ab})|+\rangle^{\otimes N}$$

were constructed, where the filtering has the same effect as taking any product initial state up to normalization. To obtain a variational class the above states were superposed in the form

$$|\Psi\rangle \propto \sum_{i=1}^{m} \alpha_i |\Psi_{\Gamma,\boldsymbol{d}^{(i)},U}\rangle,$$

where all states may differ only in their deformation vector $\boldsymbol{d}^{(i)} = \left(d_1^{(i)}, \ldots, d_N^{(i)}\right)$, while the adjacency matrix Γ and the unitary U are fixed. To test the method, the ground states of the two-dimensional Ising and XY model were approximated and compared to the exact solutions obtainable for small system sizes. The results are promising, and the method is currently generalized to higher spin systems and applied to the Bose–Hubbard model in two dimensions [12].

3. Spin chains and lattices

We consider N initially disentangled spins, embedded in a ring or d-dimensional lattice of arbitrary, but translationally invariant geometry, which interact via the Ising-type Hamiltonian, (1). The coupling strength between two spins is assumed to depend solely on the distance between them and to follow a power law $1/r^{\alpha}$ with $\alpha > 0$. We investigate relations between entanglement properties of the resulting states and these power laws. In particular, we obtain the following results:

- time-dependent states with diverging correlation and entanglement lengths in any translationally invariant d-dimensional lattice for all power laws;
- saturation of block-wise entanglement in one-dimensional chain for $\alpha > 1$;
- generalization to an area law in d dimensions, when $\alpha > (d+1)/2$;
- complete characterization of bipartite entanglement for graph states;
- dynamics of entanglement leading to random weighted graph states in equilibrium;
- random infinite weighted graph states have maximally mixed reduced density matrices for any subsystem.

3.1. Entanglement properties of weighted graph states

Throughout this section, we choose the length r_{unit} of the smallest of the vectors spanning the lattice as unit length. We consider the situation where the coupling between spins obeys a certain power law, i.e., the functions $g_{kl}(t)$ in (1), describing the strength of the coupling, only depend on the distance $r_{kl} \equiv \|k - l\|$ between particles k and l on the lattice, $g_{kl} = g(r_{kl})$ and not on time (see figure 3). As unit time we choose $g(r_{\text{unit}})^{-1}$. With these units fixed, we will express time and distance dimensionless, e.g. $t = \pi$ implicitly means $tg(r_{\text{unit}}) = \pi$. We assume that N spins are arranged on a d-dimensional lattice with some fixed, translationally invariant geometry and that all spins are initially polarized in the x-direction, i.e., their initial state is $|+\rangle^{\otimes N}$, where $|+\rangle = 1/\sqrt{2}(|0\rangle + |1\rangle)$. This initial state evolves under the interaction Hamiltonian (1) during the time $t \leqslant \pi$ into the weighted graph state $|\Psi_t\rangle$ as in (2). The restriction to times smaller than π is only technical. Later we will discuss the entanglement dynamics for all times. The states $|\Psi_t\rangle$ then become translationally invariant in the limit $N \to \infty$ or when assuming periodic boundary conditions. But our methods are not limited to translational invariant situations (see section 4).

Ising-type interactions as in (1) can occur as effective interactions. If the original interactions, from which they result, have a characteristic distance dependence, such power laws for the coupling strength arise naturally. For instance, one may consider the internal

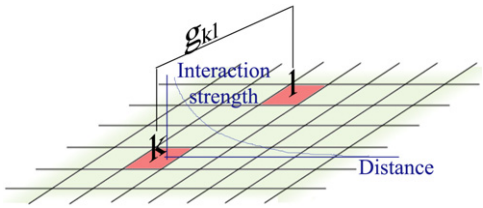

Figure 3. Illustration of a spin lattice, in which the interaction strength between two spins depends on the distance according to some power law.

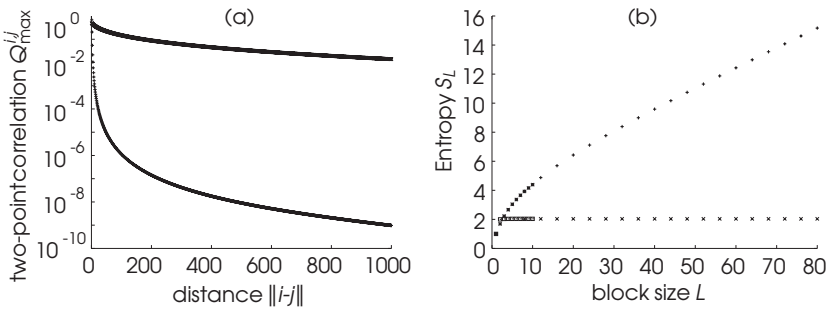

Figure 4. Spin chain with $N = 10^5, t = 0.3\pi$ and $g(r_{kl}) = r^{-1/3}$(upper curves), r^{-3} respectively (lower curves). (a) Semi-logarithmic plot of maximal two-point correlation $Q^{i,j}_{\max}$ between two particles as a function of the distance $\|i - j\|$. (b) Exact values of the entropy of entanglement S_L and upper bounds for growing block size L.

states of neutral atoms in an optical lattice that interact via some induced dipole interaction [34]. Another example are ions stored in microtraps where interactions are induced by pushing ions dependent on their internal state such that they feel a different Coulomb potential [23, 35]. The latter case leads for instance to $g(k, l) = r_{kl}^{-3}$ [35].

3.1.1. Numerical results. We apply the methods developed in section 2 to determine the entanglement properties of the state $|\Psi_t\rangle$ at a given time t for different power laws $g(r_{kl}) = r_{kl}^{-\alpha}, \alpha > 0$. Figure 4 shows the maximal two-point correlation $Q^{i,j}_{\max}$, (12), as a function of of the distance between particles $\|i - j\|$ in a one-dimensional chain of $N = 10^5$ particles. We observe that correlations decay slower than exponential. Therefore, the correlation length ξ and also the entanglement length ξ_E *diverge* [29]. This indicates long-range quantum correlations for all power laws, as we observe that only exponential fall-off functions $g(k, l) = \mathrm{e}^{-\kappa r_{kl}}$, imply a finite correlation length. We prove that long-range correlations exist for all power laws also for higher dimensional lattices in the next part.

We measure the (bipartite) entanglement between blocks L of neighbouring spins by the entropy of entanglement S_L, (10), that is the von Neumann entropy of the reduced density operator ρ_L. Note that we use the set label L instead of A as in (10) only to highlight the fact that the spins form a block. We have that $0 \leqslant S_L \leqslant L$, where $S_L = L$ indicates maximal entanglement between the blocks and the rest of the lattice. For blocks larger than 10 qubits, we make use of the strong subadditivity of the entropy to derive upper bounds on S_L according to (11).

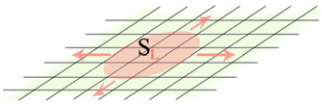

Figure 5. Illustration of L qubits contained in a d-dimensional ball. The quantity S_L is the entropy of entanglement associated with the reduced density matrix of the spins in this ball.

Figure 4(b) shows the scaling of the entropy of entanglement S_L with the block size L for different power laws. Exact values are plotted for $L \leqslant 10$, while upper bounds (corresponding to $|L_i| = 4$) are plotted for $L \geqslant 10$. The upper bound on S_L seems to grow unboundedly for $\alpha \leqslant 1/2$, whereas S_L saturates for $\alpha > 1$. We now proceed to prove the statement about saturation and comment about an indication that S_L grows unboundedly for $\alpha \leqslant 1/2$.

3.1.2. Analytical results. First, we generalize the statement about saturation of S_L in a one-dimensional chain to an area law for a d-dimensional, infinite, translationally invariant lattice. Trivially $S_L \leqslant L$ is true, and, in such a lattice, this bound translates into: S_L can at most grow like the volume of a d-dimensional ball containing L spins. Figure 5 illustrates this in two dimensions. We state the area law in the following proposition.

Proposition 1 (area law)**.** *Let L be a block of particles contained in a d-dimensional ball of radius R_L. The entropy of entanglement S_L grows for $\alpha > (1+d)/2$ at most like the surface R_L^{d-1} of the ball. For $d/2 < \alpha \leqslant (1+d)/2$, the entropy S_L grows at most like $R_L^{2(d-\alpha)} \ln(R_L)$, and for $\alpha = (d+1)/2$ like $R_L^{d-1} \ln^2(R_L)$. For $\alpha \leqslant d/2$, our bounds give no growth restriction other than the trivial growth with the volume R_L^d.*

For the proof we need the following proposition.

Proposition 2 (one spin in d dimensions)**.** *If $\alpha > d/2$ the entropy of entanglement S_1 of one spin is smaller than 1, otherwise it is 1.*

Proof. In a translationally invariant lattice, all reduced density operators of one qubit are the same, since the functions g in (1) only depend on the distance between the qubits. Hence, without loss of generality, we pick the qubit at the origin whose reduced density operator in the computational basis is $\rho_0 = \frac{1}{2}[\mathbb{1} + c|0\rangle\langle 1| + c^*|0\rangle\langle 1|]$ with $c = \prod_{\boldsymbol{k}} \left[\cos\frac{\varphi_{0\boldsymbol{k}}}{2}\, \mathrm{e}^{-\mathrm{i}\varphi_{0\boldsymbol{k}}/2}\right]$ and $\varphi_{0\boldsymbol{k}} \propto r_{0\boldsymbol{k}}^{-\alpha} = |\boldsymbol{k}|^{-\alpha}$. The infinite product is said to converge if and only if $\sum_{\boldsymbol{k}} \ln\left[\cos\frac{\varphi_{0\boldsymbol{k}}}{2}\, \mathrm{e}^{-\mathrm{i}\varphi_{0\boldsymbol{k}}/2}\right] = \sum_{\boldsymbol{k}} \left[\ln\cos\frac{\varphi_{0\boldsymbol{k}}}{2} - \mathrm{i}\varphi_{0\boldsymbol{k}}/2\right]$ converges. Since the first summand is purely real and the second purely imaginary, $\sum_{\boldsymbol{k}} \ln\cos|\boldsymbol{k}|^{-\alpha}$ and $\sum_{\boldsymbol{k}} |\boldsymbol{k}|^{-\alpha}$ must converge independently.

If $f : [1, \infty[\to \mathbb{R}_0^+$ is monotonously falling then Cauchy's integral criterion says that $\sum_{j=1}^{\infty} f(j)$ converges if and only if $\int_1^{\infty} f(x)\,\mathrm{d}x < \infty$ (in the sense of an improper Riemann integral). Here, we have $\ln\cos|\boldsymbol{k}|^{-\alpha}$ in the first sum which is monotonously increasing for $k \geqslant 1$ from negative values. Hence, by adding an overall negative sign we can apply Cauchy's integral criterion, and, in d dimensions, $\sum_{\boldsymbol{k}} \ln\cos|\boldsymbol{k}|^{-\alpha}$ converges if and only if $-\int_1^{\infty} \ln\cos x^{-\alpha} x^{d-1}\,\mathrm{d}x < \infty$, where we used polar coordinates and implicitly performed the trivial angular integrations. We put bounds on the integrand in the following way:

$$\begin{aligned}\frac{x^{-2\alpha}}{2} - \frac{x^{-4\alpha}}{24} &\leqslant -\ln\left(1 - \frac{x^{-2\alpha}}{2} + \frac{x^{-4\alpha}}{24}\right) \leqslant -\ln\cos x^{-\alpha} \\ &\leqslant -\ln\left(1 - \frac{x^{-2\alpha}}{2}\right) \leqslant \frac{x^{-2\alpha}}{2} + x^{-3\alpha}\end{aligned}$$

for all $x \in [1, \infty[$. Using the upper bound, $\int_1^\infty (x^{-2\alpha}/2 + x^{-3\alpha})\,\mathrm{d}x < \infty$ implies $\prod_{\boldsymbol{k}} \cos|\boldsymbol{k}|^{-\alpha} > 0$, which is the case for $\alpha > d/2$. Using the lower bound, $\int_1^\infty (x^{-2\alpha}/2 - x^{-4\alpha}/24)\,\mathrm{d}x = \infty$ implies $\prod_{\boldsymbol{k}} \cos|\boldsymbol{k}|^{-\alpha} = 0$, which is the case for $\alpha \leqslant d/2$.

In d dimensions the second sum describing the phase converges if $\int_1^\infty x^{-\alpha} x^{d-1}\,\mathrm{d}x < \infty$ by Cauchy's integral criterion (using again polar coordinates and implicitly performing the trivial angular integrations). The integral is finite for $\alpha > d$, a stricter condition than before, and in [7] proposition 1 was stated only for $\alpha > d$. However, the entropy of entanglement S_1 can be computed from the eigenvalues $\frac{1+|c|}{2}$, $\frac{1-|c|}{2}$ of ρ_0 where the phase part of c is absent, and the question is whether the phase is necessary at all.

We will show that the reduced density matrix of one qubit may not exist if we go to the limit of infinitely many qubits, but that the limit of single qubit entropies does exist. Around the qubit 0 at the origin of the d-dimensional lattice we lay a hypersphere B_R of radius $R \in \mathbb{N}$ within which the lattice sites are filled with qubits while they are empty outside. The translationally invariant limit is reached when $R \to \infty$. The reduced density matrices $\left(\rho_0^R\right)_{R=1}^\infty$ for qubit 0 form a sequence, each element of which is the reduced density matrix of finitely many qubits. For finitely many qubits the modulus and phase of c_R can be written as $\prod_{\boldsymbol{k}\in B_R} \cos\frac{\varphi_{0\boldsymbol{k}}}{2}$ and $\mathrm{e}^{-\mathrm{i}/2\sum_{\boldsymbol{k}\in B_R}\varphi_{0\boldsymbol{k}}}$ respectively. Both modulus and phase of c_R are finite real numbers. When we know the phase we can perform the basis change to the eigenbasis (the eigenvectors depend on the phase of c_R), and compute the entropy of entanglement S_1^R, which is a continuous function of $|c_R|$ and also of c_R. When we take the limit $R \to \infty$ three cases can arise. First, if $\alpha \leqslant d/2$ the modulus converges to zero, and hence c_R converges to zero (even if the phase diverges), which leads to the uninteresting case $S_1 = 1$. Second, if $\alpha > d$ both modulus and phase converge independently to a finite value larger than zero (which implies that they also converge jointly). In this case, the reduced density matrix is well defined and so is the transformation to the eigenbasis. The entropy of entanglement is now nontrivial, $S_1 < 1$. Third, if $d/2 < \alpha \leqslant d$ the modulus converges to a finite value larger than zero, but not the phase, which is infinite. In this case, the reduced density matrix looks ill-defined in the computational basis. Viewed in the eigenbasis the matrix seems well defined, but we do not know how to transform to the eigenbasis, since the eigenvectors now contain the phase '$\mathrm{e}^{\pm\mathrm{i}\infty}$'. We sidestep the problem with $\lim_{R\to\infty}\left(\rho_{\boldsymbol{0}\boldsymbol{k}}^R\right)_1^\infty$ and simply define the entropy of entanglement S_1 as the limit $\lim_{R\to\infty} S_1^R$ of the well-defined sequence elements S_1^R. Then, S_1 is again smaller than 1, and, in this sense, we have proved the proposition. □

If we want to choose fall-off functions other than negative powers we can decide convergence by comparing them to the critical power function $x^{-d/2}$.

Proof of proposition 1. Be $\alpha > d/2$, and let the origin of the lattice coincide with the centre of the sphere B_{R_L} of radius R_L containing L qubits. Let $r := R_L - |\boldsymbol{k}|$ be the distance of some qubit at lattice site $\boldsymbol{k}$ to the surface of the sphere. We define

$$S(\rho_1|r) := -\left[\frac{1}{2}(1+b_r)\log_2\frac{1+b_r}{2} + \frac{1}{2}(1-b_r)\log_2\frac{1-b_r}{2}\right]$$

with $b_r := \prod_{\boldsymbol{m}\notin\bar{B}_r}\cos(|\boldsymbol{m}|^{-\alpha})$, where $\bar{B}_r$ is the closed sphere of radius r around some lattice site $\boldsymbol{k}$, for which $R_L - |\boldsymbol{k}| = r$. We omitted the phase in the definition of b_r, otherwise one would have to write absolute values in the above formula (see also the discussion in the proof of proposition 2). The quantity $S(\rho_1|r)$ is the entropy of entanglement for a 1-qubit reduced density matrix which is shielded from the influence of other qubits that are within a radius r (see figure 6).

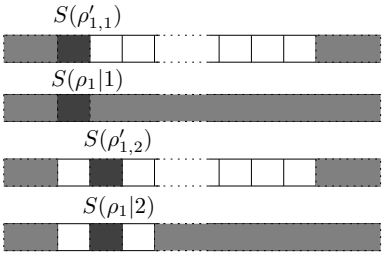

Figure 6. Illustration of how the entropies $S(\rho_{L_i})$ are replaced by larger entropies $S(\rho_1|i)$ in the computation of an upper bound on $S(\rho_L)$.

Let $\sum_{\boldsymbol{k}\in B_{R_L}} S(\rho'_{1,\boldsymbol{k}})$ be the reduced density matrix of one qubit at site $\boldsymbol{k}$ derived from ρ'_L. We use the subadditivity of S_L for the following inequality:

$$S(\rho_L) = S(\rho'_L) \leqslant \sum_{\boldsymbol{k}\in B_{R_L}} S(\rho'_{1,\boldsymbol{k}}) \leqslant \sum_{\boldsymbol{k}\in B_{R_L}} S(\rho_1|r). \tag{14}$$

For a nontrivial upper bound we must determine whether the shielding for large r is sufficiently large, so we need to put lower bounds on b_r retaining the correct scaling of b_r for large r. Cauchy's integral criterion tells us that for any real function $f < 0$, for which the infinite sums converge, $\sum_{k=k_0+1}^{\infty} f(k) \geqslant \int_{k_0}^{\infty} f(x)\,\mathrm{d}x \geqslant \sum_{k=k_0}^{\infty} f(k)$. Hence, we can rewrite $b_r = \mathrm{e}^{\sum_{m\notin \bar{B}_r} \ln\cos|\boldsymbol{m}|^{-\alpha}}$ and compare the exponent to an integral using again polar coordinates (with trivial angular integrations),

$$\begin{aligned}\int_r^{\infty} \ln(\cos x^{-\alpha}) x^{d-1}\,\mathrm{d}x &\geqslant \int_r^{\infty} \ln\left(1-\frac{x^{-2\alpha}}{2}\right) x^{d-1}\,\mathrm{d}x \\ &\geqslant -\frac{1}{2}\int_r^{\infty} x^{-2\alpha} x^{d-1}\,\mathrm{d}x - \int_r^{\infty} x^{-3\alpha} x^{d-1}\,\mathrm{d}x.\end{aligned}$$

The last integral is larger than, say, $1/2$ for all r larger than some r_0, so b_r scales at least like $\mathrm{e}^{-r^{d-2\alpha}/2}$ for $r > r_0$.

Now, we can determine the scaling of $\sum_{\boldsymbol{k}\in B_{R_L}} S(\rho_1|r)$. Note that in the formula for $S(\rho_1|r)$ the second term, $-(1-b_r)/2\log_2[(1-b_r)/2]$, is always larger than the first. Consequently it is enough to study the scaling of this second term for large r, and we consider the natural logarithm instead of the binary logarithm. We find $\ln[(1-b_r)/2] = -\ln(r^{d-2\alpha}) + \mathcal{O}(1)$. To leading order we have

$$-(1-b_r)/2\ln[(1-b_r)/2] = -r^{d-2\alpha}\ln(r^{d-2\alpha}) + \mathcal{O}(r^{(d-2\alpha)}).$$

To compute the scaling of $\sum_{\boldsymbol{k}\in B_{R_L}} S(\rho_1|r)$ we use the above relation, Cauchy's integral criterion and polar coordinates and obtain the integral $-\int_c^{R_L} x^{d-2\alpha}\ln(x^{d-2\alpha})(R_L-x)^{d-1}\,\mathrm{d}x$, where we put some constant c as the lower integration limit. Technically we must demand $c > r_0$, but c is unimportant for the scaling, and we can allow to assign an arbitrary value to c, namely the one that gives the easiest expressions. The choice $c = 1$ and binomial expansion of $(R_L - x)^{d-1}$ lead to

$$\begin{aligned}&\sum_{k=0}^{R_L}(-1)^k\binom{R_L}{k} R_L^{d-1-k}\int_1^{R_L}(-1)x^{d-2\alpha}\ln(x^{d-2\alpha})x^k\,\mathrm{d}x \\ &\quad= \sum_{k=0}^{R_L}(-1)^k\binom{R_L}{k}\frac{(2\alpha-d)\big[\big((d+k-2\alpha+1)\ln(R_L)-1\big)R_L^{2(d-\alpha)} + R_L^{d-1-k}\big]}{(d+k-2\alpha+1)^2}.\end{aligned} \tag{15}$$

The denominators in the above summands could cause problems for $\alpha \to (d+1+k)/2$. But there are no poles in the fractions since

$$\lim_{\alpha\to(d+1+k)/2} \frac{(2\alpha-d)\left[\left((d+k-2\alpha+1)\ln(R_L)-1\right)R_L^{2(d-\alpha)}+R_L^{d-1-k}\right]}{(d+k-2\alpha+1)^2} = \frac{1}{2}(1+k)R_L^{d-1-k}\ln^2(R_L). \tag{16}$$

For $d/2 < \alpha \leqslant (d+1)/2$, the highest order in (15) is $R_L^{2(d-\alpha)}\ln(R_L)$ (present in all summands), while for $\alpha = (d+1)/2$ the term with $k=0$ dominates and, by (16), has the scaling behaviour $R_L^{d-1}\ln^2(R_L)$. Both cases do not occur for $d=1$ since they would violate $\alpha > d/2$. For $\alpha > (d+1)/2$, the highest order is R^{d-1}, which occurs in the term with $k=0$. Note that the respective highest orders come with positive numerical factors as they should. Finally, for $\alpha \leqslant d/2$, there exists no shielding, $S(\rho_1|r)=1$ for all qubits, and summation leads only to the trivial scaling R_L^d. □

Now, we prove the following statement about 2-point correlations.

Proposition 3 (long-range correlations)**.** *For all power laws, the maximal two-point correlation $Q_{\max}^{k,l}$, see equation (12), decays slower than exponential as a function of the distance $n := \|k-l\|$ between particles k, l in any d-dimensional, translationally invariant lattice.*

Proof. Let $\psi = n^{-\alpha}$ be the phase between qubits k, l, where, technically, we choose the time $t=1$ (any finite time would be just as good, but could necessitate technical modifications). The set of all lattice sites be V, and we define

$$C_k := \prod_{a\in V}\cos\frac{\varphi_{ka}}{2}, \qquad C'_k := \left(\prod_{a\in V}\cos\frac{\varphi_{ka}}{2}\right)\left(\cos\frac{\psi}{2}\right)^{-1}$$
$$\Phi_k := \sum_{a\in V}\varphi_{ka}, \qquad \Phi'_k := -\psi + \sum_{a\in V}\varphi_{ka}$$
$$C'_{l-k} := \prod_{a\in V, a\neq l,k}\cos\frac{\varphi_{la}-\varphi_{ka}}{2}$$
$$C'_{l+k} := \prod_{a\in V, a\neq l,k}\cos\frac{\varphi_{la}+\varphi_{ka}}{2}.$$

According to (8) and (9) and exploiting the symmetry between qubits k, l, the reduced density matrix of qubits k, l is

$$\rho_{k,l} = U(\psi)\rho'_{k,l}U^\dagger(\psi) = 1/4\begin{pmatrix} 1 & \mathrm{e}^{-\frac{\mathrm{i}\Phi'_k}{2}}C'_k & \mathrm{e}^{-\frac{\mathrm{i}\Phi'_k}{2}}C'_k & \mathrm{e}^{-\mathrm{i}\psi-\mathrm{i}\Phi'_k}C'_{k+l} \\ \mathrm{e}^{\frac{\mathrm{i}\Phi'_k}{2}}C'_k & 1 & C'_{l-k} & \mathrm{e}^{-\mathrm{i}\psi-\frac{\mathrm{i}\Phi'_k}{2}}C'_k \\ \mathrm{e}^{\frac{\mathrm{i}\Phi'_k}{2}}C'_k & C'_{l-k} & 1 & \mathrm{e}^{-\mathrm{i}\psi-\frac{\mathrm{i}\Phi'_k}{2}}C'_k \\ \mathrm{e}^{\mathrm{i}\psi+\mathrm{i}\Phi'_k}C'_{k+l} & \mathrm{e}^{\mathrm{i}\psi+\frac{\mathrm{i}\Phi'_k}{2}}C'_k & \mathrm{e}^{\mathrm{i}\psi+\frac{\mathrm{i}\Phi'_k}{2}}C'_k & 1 \end{pmatrix}.$$

Any 2-point correlation is a lower bound to the maximal 2-point correlation. Moreover, assume that only one 2-point correlation is different from zero, then $Q_{\max}$ would equal the absolute value of that correlation. In a full correlation matrix, the absolute value of any

correlation is hence a lower bound for $Q_{\max}$. In our case, we compute the 2-point correlation $Q_{xz} = C_k \sin\frac{\Phi_k}{2} \tan\frac{\psi}{2}$, and since $\psi \in]0, 1]$ we have[4]

$$Q^{k,l}_{\max} \geqslant \left| C_k \sin\frac{\Phi_k}{2} \right| \tan\frac{\psi}{2}.$$

Let α be larger than d. By proposition 2 we have $\left|C_k \sin\frac{\Phi_k}{2}\right| = \text{constant}$, and since $\tan\frac{\psi}{2}$ falls off like $\psi = n^{-\alpha}$ for large n, the maximal 2-point correlation function falls off slower than $n^{-\alpha}$, i.e., slower than exponential.

For $d/2 < \alpha \leqslant d$, we run into the same subtleties as in the proof of proposition 2 since $\Phi_k = \infty$. As a limit of well-defined sequences, one can still establish the result based on Q_{xy} as above. However, for the claim that correlations fall off slower than exponential for all power laws, the high powers are significant anyways, so we do not go into details. In the same spirit we merely note that $Q_{\max} = 1/2C'_{l-k}$ for $0 < \alpha \leqslant d/2$, which can also be shown to fall off slower than exponential. Interestingly, for some fixed distance n between qubits k, l, the maximal 2-point correlation need not fall off monotonically with α. There can be a local maximum around the value $\alpha \approx d/2$. □

3.1.3. Numerical issues with infinite lattices. To numerically compute exact values or upper bounds, one cannot sum or multiply infinitely many terms. But if one sums/multiplies only finitely many terms, one gets values for the entropy that are lower than the correct values for an infinite chain because of the properties of the Hadamard product used to construct the reduced density matrices (see our earlier discussion on this topic in section 2). In this way it could happen that the true value of the entropy S_L might actually be higher than the value of the 'upper bound' computed in a finite lattice. In practice this is not the case. By using the strong subadditivity we overestimate the value for S_L much more than we underestimate it by not summing to infinity, but only to a reasonably large number k_0. Here, the criterion for k_0 to be 'reasonably large' depends on how fast the function $g(k, l)$ in (1) falls off. Still, to be on the safe side, we want to control the error. When we compute some matrix element in a reduced density matrix, there are two possibilities. Either, the infinite product does not converge, i.e., we obtain the trivial value zero, in which case this is the exact value for the infinite chain, or the product converges to a nonzero value. In the latter case, we can estimate the sum of summands we left out by the integral related to it via Cauchy's integral criterion. Remember that, in one dimension and for any real function $f < 0$ the relation $\sum_{k=k_0+1}^{\infty} f(k) \geqslant \int_{k_0}^{\infty} f(x)\,\mathrm{d}x \geqslant \sum_{k=k_0}^{\infty} f(k)$ holds. In higher dimensional lattices one would have to use the appropriate (polar) integration measures in the integrals.

As an example, let us consider the reduced density operator of one qubit in a doubly infinite chain. We assign the position 0 to this qubit and we look at the interesting case $\alpha > 1/2$. Remember that the off-diagonal element is then $c = \left[\prod_{k=1}^{\infty}\left(\cos\frac{k^{-\alpha}}{2}\right)^2\right] \mathrm{e}^{-2\mathrm{i}\sum_{k=1}^{\infty} k^{-\alpha}/2}$ and the square is necessary since we deal with a doubly infinite chain. Again, we will omit the phase part having in mind the discussion in the proof of proposition 2. Suppose we have calculated $c_{\text{num}} := \prod_{k=1}^{k_0}\left(\cos\frac{k^{-\alpha}}{2}\right)^2$. Now, we try to put a lower bound on $\prod_{k=k_0+1}^{\infty}\left(\cos\frac{k^{-\alpha}}{2}\right)^2 = \mathrm{e}^{2\sum_{k=k_0+1}^{\infty}\ln\cos(k^{-\alpha}/2)}$. We choose k_0 large such that $\cos(k^{-\alpha}/2) \approx 1 - \frac{1}{8}k^{-2\alpha}$. (The approximation is strictly a '$\geqslant$', which is what we want.) Then we form $\int_{k_0}^{\infty}\ln\left(1 - \frac{1}{8}x^{-\alpha}\right)\mathrm{d}x \geqslant \frac{1}{2\alpha-1}k_0\ln\left(1 - \frac{1}{8}k^{-(2\alpha-1)}\right)$. With this result, we find a factor $c_\infty := \exp\left\{\frac{2}{2\alpha-1}k_0\ln\left(1 - \frac{1}{8}k^{-(2\alpha-1)}\right)\right\}$ such that $c_{\text{num}} \geqslant |c| \geqslant c_\infty c_{\text{num}}$. When we use this last

[4] The last statement is true when we choose the shortest vector that spans the translationally invariant lattice to have unit length.

expression to compute the entropy for the 1-qubit reduced density matrix (or use this entropy further to derive bounds for larger blocks) we will end up with true upper bounds.

In principle, one can do the same thing for every entry in any reduced density matrix. Suppose we have computed a reduced density matrix $\rho_{L,\mathrm{num}}$ and a matrix $\rho_{L,\infty}$ containing factors between 0 and 1 (like the above c_∞) representing corrections for all the left-out parts. When we form the Hadamard product of these two matrices, then theorem 5.5.12 in [24] again tells us that we have truly got an upper bound on the entropy. The procedure to obtain the values of $\rho_{L,\infty}$ is very tedious. Usually, it is not necessary to be that strict because the matrix $\rho_{L,\mathrm{num}}$ is already an excellent approximation when k_0 is chosen appropriately. In our numerical calculations we had $k_0 \approx 10^5$, which is large enough for the smallest power we used, namely $\alpha = -1/3$.

3.1.4. Graph states. In the previous discussion of this section we have seen that upper bounds on the entropy of entanglement of some block of qubits in d-dimensional lattices exist. However, without a lower bound on the same quantity, we have not shown that the scaling of the true value of the entropy does scale *at least* like, say, the surface. In principle, the entropy could still saturate for all power laws.

For graph states, we can get a complete analytic description of the entanglement properties and show that there are indeed states in the class of weighted graph states where the entanglement does not saturate.

In the following, we consider the case where the interaction Hamiltonian has a fixed interaction length λ and constant interaction strength, i.e., $g(r_{kl}) = 1$ if $r_{kl} \leqslant \lambda$ and zero otherwise. For $t = \pi$, the resulting states $|\Psi_\pi\rangle$ are instances of graph states [15, 16]. We denote a d-dimensional quadratic block of size $L = a^d$ neighbouring spins by A and the remaining system by B. Again, we measure the bipartite entanglement between A and B by the entropy of entanglement S_L.

For the graph states, the reduced density matrices are straightforwardly calculated. The special value π for the phases simply makes matrix entries vanish. Consider an infinite chain and a block of L qubits in this chain. If $\lambda \geqslant L/2$ then the reduced density matrix of the L qubits is the identity, hence $S_L = L$. If $\lambda < L/2$ then some qubits in the block are not connected to any qubit outside of the block (and connections within the block can be neglected for the entropy). These qubits can be completely ignored since they do not contribute to the entropy. The number of qubits that have connections to qubits outside of the block is 2λ. The reduced density matrix of these 2λ qubits is again the identity, and the entropy is $S_L = 2\lambda$. Putting the two cases together we can write $S_L = \min(2\lambda, L)$. It is straightforward to generalize to higher dimensions or to choose only a finite environment of qubits. We will not discuss theses cases in terms of our PEPs reduced density matrices because, for graph states, there is a very elegant algebraic approach [36].

For graph states, S_L is given by the binary rank, i.e., the rank modulo 2, of the adjacency matrix Γ_{AB} between the quadratic block A and the rest B [36]. If the lattice is large enough to contain not only the block A but also the larger block of size $(a + 2\lambda)^d$ with A in its centre, then no boundary effects have to be taken into account. We can inductively show that the matrix Γ_{AB} has maximal rank by considering different layers A_k with geometric distance k to B, starting with $k = 1$. Hence, S_L is simply given by the number of vertices within A that are connected to the rest B, that is $S_L = a^d - [a - \min(2\lambda, a)]^d$ with $a = \sqrt[N]{L}$. In a general situation, no such simple rule to calculate S_L holds.

A counterexample is given by a state with $N = 4$, $\varphi_{13} = \varphi_{14} = \varphi_{23} = \varphi_{24} = \pi$, which is maximally connected graph and has $S(\rho_{12}) = 1$. Simply counting the connections would lead to the answer $S(\rho_{12}) = 2$ (the maximal entropy). For an (infinite) chain of particles we

obtain $S_L = \min(2\lambda, L)$. As L increases, S_L saturates at the value 2λ for any fixed interaction length λ. Only if λ itself goes to infinity as $N \to \infty$, S_L can grow (unboundedly) with L when the ratio of the interaction length to the total number of particles is kept constant. For a given interaction length λ, and for any ball containing L particles, only those particles, that have connections to the remaining system, contribute to S_L. The entropy S_L equals L if the radius of the hypersphere is smaller than λ. Otherwise, S_L scales essentially like the volume of a surface shell with thickness λ , that is $S_L \propto \lambda L^{(d-1)/d}$. Two-point correlation functions $Q^{i,j}_{\alpha,\beta}$ turn out to be zero for all pairs of particles (except for the case of two neighbouring particles at the end of a chain), because their reduced density matrix ρ_{kl} is the identity [36]. Nevertheless, $|\Psi_\pi\rangle$ is maximally connected [15, 16], which means that a Bell state between any pair of particles can be obtained by local measurements on the rest of the particles. Hence $|\Psi_\pi\rangle$ has maximal localizable entanglement between any two particles, $E_L = 1$, and, thus, an infinite entanglement length. Finally, we remark that $E_{MW} = 1$ for all such states since the reduced density operator of each single particle is also the identity.

The question remains whether graph states are exceptional in the class of weighted graph states concerning entanglement properties, or whether other weighted graph states show similar or even higher entropy scaling. In the following subsection we will see that, indeed, almost all weighted graph states display an entropy scaling with the volume.

3.2. Entanglement dynamics and random weighted graph states

We return to a d-dimensional lattice and to Hamiltonians with arbitrary distance dependence $g(\boldsymbol{k}, \boldsymbol{l}) = r_{\boldsymbol{kl}}^{-\alpha}$ and consider the *dynamics* of entanglement, that means the change of entanglement and correlations of the (infinite) weighted graph state $|\Psi_t\rangle$ with time. The scaling of the entropy with block size L is essentially still governed by the specific form of the distance dependence for any finite t because infinitely remote regions still influence a subsystem in a similar way as discussed before.

For large times t, more and more of the interaction phases $\varphi_{kl} = g(\boldsymbol{k}, \boldsymbol{l})t$ start to oscillate (as they are effectively taken modulo π because of the cos-/phase-functions). In the limit of large t, the phases are distributed in the interval $[0, 2\pi[$ according to a (quasi)-random distribution. When we consider the off-diagonal elements of reduced density operators in this limit, we see that they all contain infinite products of cosines of (sums of) *random* angles. Hence, all these products are zero and lead to a maximally mixed state, which suggests the following proposition.

Proposition 4 (long-time limit)**.** *In an infinite d-dimensional lattice and in the long-time limit $t \to \infty$, the entropy of the reduced density operator of any finite group A of particles is maximal, $S(\rho_A) = |A|$.*

The intuitive way described above to understand the proposition is certainly correct, but for a rigorous proof we must keep in mind that we do not have true random angles at any finite time, and we cannot use a time $t = \infty$ at which the statement about the randomness of the phases would correct. The statement $S(\rho_A) \to |A|$ for $t \to \infty$ is still correct, but the proof does, indeed, rely on the actual deterministic values of the phases and not on randomness.

Proof of proposition 4. The phase parts of all matrix entries can be neglected for this proof, since they do not matter once we can show that the moduli vanish. We start with a 1-qubit reduced density matrix and later extend the argument to any ρ_A. The off-diagonal matrix entry is $|c(t)| = \prod_k \cos \frac{t}{2|\boldsymbol{k}|^\alpha}$. It turns out to be enough to pick a one-dimensional, one-sided chain containing the qubit 0 for which we calculate the reduced density matrix. We label the other

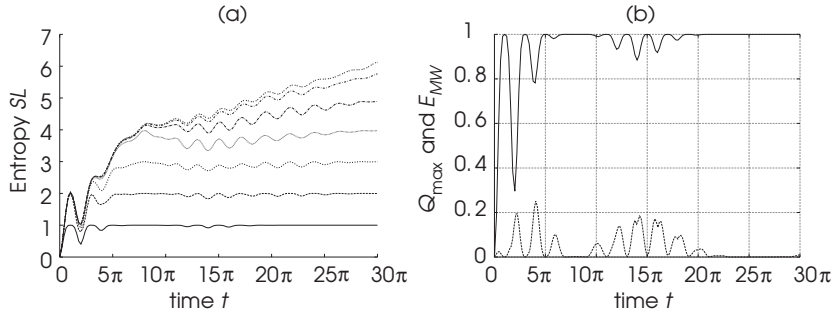

Figure 7. (a) Dynamics of entanglement for chain with $N = 10^5$ and $g(r_{kl}) = r_{kl}^{-3}$. Entropy of entanglement S_L for blocks up to $L = 7$. (b) Dynamics of maximal 2-point correlation function $Q_{\max}^{k,l}$ for $\|k - l\| = 5$ (lower curve) and Mayer–Wallach entanglement measure E_{MW} (upper curve).

qubits by j, where $j = 1, 2, \ldots$, and we want to show $\lim_{t\to\infty} \prod_{j=1}^{\infty} \cos \frac{t}{2j^\alpha} = 0$. We ask, at a fixed time T, how many of the cos-factors are smaller than $1 - \varepsilon$ for some ε? Certainly, there are many factors fulfilling this, which have already begun to oscillate, but they are hard to evaluate, and we will not need them. So we completely neglect the oscillatory part on which we had based the intuitive approach to the statement we want to prove. We choose $\varepsilon = 1/2$, and we determine the number N_j of factors which have left the ε-environment of 1 for the first time and, for simplicity, are larger than zero. The conditions we want to meet are $0 < \cos \frac{T}{2j^\alpha} < 1/2$ which is equivalent to $j < \left(\frac{3T}{2\pi}\right)^{1/\alpha}$ and $j > \left(\frac{T}{\pi}\right)^{1/\alpha}$. So the number $N_j \approx \left\lfloor \left(\frac{3T}{2\pi}\right)^{1/\alpha} - \left(\frac{T}{\pi}\right)^{1/\alpha} \right\rfloor$. For all $\alpha \in]0, \infty[$ this number N_k goes to infinity as $T \to \infty$. Hence, $\lim_{T\to\infty} \prod_{k=1}^{\infty} \cos \frac{T}{2k^\alpha} = 0$, the matrix becomes the identity and the entropy of entanglement is maximal, i.e., 1 in the 1-qubit case. To complete the proof we state that arbitrary off-diagonal matrix elements in any reduced density operator vanish by the same arguments. The only difference is the following. The vanishing need not happen at the same speed for all entries in the matrix since cancellations in some orders of α can occur. Naturally, this fact is not important for the asymptotic statement. □

From the formula for the N_j we see that the larger the exponent α is, the slower the entropy will asymptotically reach its maximal value. In between, it can (and will) oscillate. The oscillations are damped which again can be seen from the growing number of N_j. The maximal value will be attained again and again as time evolves (e.g. in the 1-qubit case this happens whenever some phase is exactly π). For a chain of $N = 10^5$ particles with $g(r_{kl}) = r_{kl}^{-3}$ the time dependence of the entropy of entanglement for blocks up to size 7 is plotted in figure 7(a).

Figure 7(b) shows how the maximal two-point correlation function $Q_{\max}^{k,l}$ decays over time (here for $\|k - l\| = 5$) while the Meyer–Wallach entanglement measure E_{MW} approaches 1 in a kind of mirrored version. This behaviour is easy to understand: when there is maximal entanglement, i.e., maximal quantum correlations, then the classical correlations are at a minimum and vice versa.

To conclude the section we formulate a proposition about truly random weighted graph states, which is motivated by the discussion above. We call those weighted graph states truly random, for which the interaction phases between any two spins are drawn from some probability distribution. In the following proposition we explicitly want to exclude those

discrete distributions, for which the differences between any two of the random variable values are integer multiples of 2π. Only for such discrete distributions some off-diagonal matrix entries C_{s_A,s'_A} of an arbitrary, finite reduced density matrix, compare equation (9), can be nonzero, because then possibly $\prod_{k=1}^{\infty}\cos\left[\frac{1}{2}(s_A - s'_A)\cdot\Gamma_k\right] \neq 0$. In all other cases, this product will be zero for $s_A \neq s'_A$ since it will contain infinitely many factors that are smaller than one.

Proposition 5 (random weighted graph states)**.** *In an infinite, random weighted graph state the entropy of the reduced density operator of any finite group A of particles is maximal,* $S(\rho_A) = |A|$. *Since non-random weighted graph states are untypical states in the class, the proposition can be rephrased to read: for almost all infinite weighted graph states the entropy of the reduced density operator of any finite group A of particles is maximal.*

Random weighted graph states naturally arise in the context of irregular systems like spin glasses or spin gases. To the latter we turn our attention now.

4. Spin gases

A *spin gas* is a natural extension of a classical gas. It consists of a large number of interacting particles whose (random) motion is described classically, while additional internal (quantum mechanical) degrees of freedom are taken into account. In general, we define a spin gas as a system of interacting spins (or qubits) where the coupling strengths between the spins are stochastic functions of time. In this respect they differ from the spin lattices of the previous section, and, in fact, they are more closely related to spin glasses, which have random, albeit static, couplings between the spins. Although there has been much recent work investigating e.g. the role of entanglement in quantum critical phenomena [29, 37–41], there is little theoretical work studying disordered quantum systems such as spin glasses and spin gases from a similar perspective (see, however, [42, 43]).

In full generality, a spin gas seems intractable for various reasons: the description of a many-body quantum state usually requires exponentially large resources; strong interactions do not allow for a perturbative treatment; random interactions prevent the appearance of symmetries and the corresponding reduction of the effective number of degrees of freedom; finally, the restriction to low-energy eigenspaces, suitable for the study of ground-state or low-temperature properties, cannot be applied here to the study of dynamics. Similarly as in proposition 9 entanglement will usually grow with the volume of any sub-system of spins, and hence DMRG and related methods are expected to fail. Here, we will circumvent these problems by using a weighted graph state model, where computations are possible although the amount of entanglement involved can be arbitrarily large. Let $(|+\rangle^{\otimes N})$ again describe the internal state of the gas particles initially. This product state evolves under the interaction Hamiltonian (1)—leading to a weighted graph state. In this way we can apply the whole formalism developed in section 2. In contrast to the spin lattices, the coupling functions g will now depend on time in a way determined by the collisions of the (semi-classical) particles.

In other words, we analyse how the evolution of the quantum state and its entanglement properties are determined by the underlying classical kinematics of the gas for an exact microscopic model. Spin gases are therefore interesting both from the perspective of thermodynamics and of quantum information.

We point out here, that we describe the systems by pure states, albeit with random coefficients, and calculate expected properties by averaging them over different instances of these states. We concentrate on two different kinds of gases. The first is the semi-

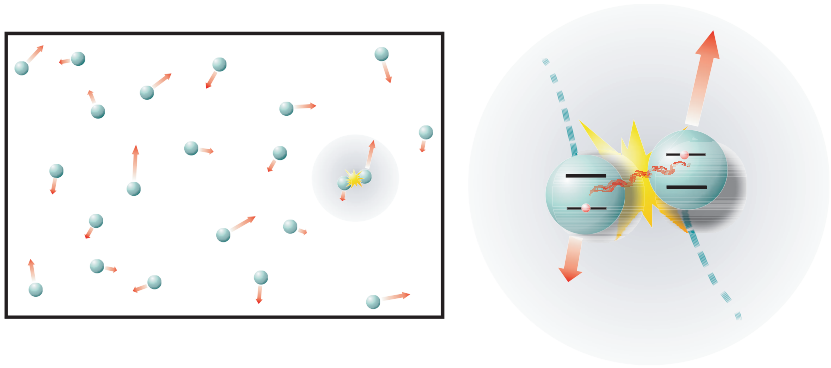

Figure 8. Semi-quantal Boltzmann gas in a box. Collisions lead to interactions of internal (quantum) degrees of freedom of the particles.

quantal Boltzmann gas, where each particle carries an internal (two-level) quantum degree of freedom. During a collision of two particles, the internal degrees of freedom interact and can become entangled (see figure 8). Here, the statistics of the collisions, described by kinetic gas theory, leads to the randomly fluctuating coupling strengths between the spins. For a dilute gas, where the mean free path is so large that neighbourhood relations do not play a role, we analytically calculate the rate at which entanglement is produced and characterize the entanglement properties of the equilibrium state.

The second is a lattice gas, where the gas particles do not move freely in space, but are confined to lattice sites, between which they can classically hop with a certain probability and interact when they are nearest neighbours. Such a system could be realized e.g. by neutral atoms hopping in an optical lattice.

We present the following results.

- Boltzmann gas:
  - initial entanglement generation rate $\propto \sqrt{T}$ at low temperatures (large collision phases) and $\propto \sqrt{T^{-1}}$ at high temperatures (small collision phases);
  - entropy of entanglement in equilibrium at most one ebit away from the maximal value for any subsystem.
- Lattice gas:
  - formation of clusters: maximal distance between localizable entangled pairs grows exponentially with time;
  - entanglement dynamics strongly depends on geometry of the setup, e.g. on initial positions of the subsystem spins in the lattice;
  - lattice gas has memory: correlated and uncorrelated collision events can be distinguished.

4.1. Boltzmann gas

We consider a dilute ideal gas of N particles in thermal equilibrium with a mean free path comparable to the size of the enclosing volume. The statistical state of the gas is fully specified by the density n, the volume V, and the temperature T. We assume Stoßzahlansatz (or molecular chaos) and hence take a homogeneous and uncorrelated spatial distribution of the particles (density), and an uncorrelated velocity distribution. The latter is given by the

Maxwell–Boltzmann distribution

$$p(\vec{\mathrm{v}}) = (2\pi\sigma^2)^{-3/2}\exp[-\mathrm{v}^2/(2\sigma^2)], \tag{17}$$

which is characterized by the single parameter $\sigma = \sqrt{k_B T/m}$, where m is the mass of the particles and k_B the Boltzmann constant. We further assume a hard-sphere model for collisions between particles of diameter d. During a collision two particles k and l acquire a phase inversely proportional to their momentary relative velocity, $\varphi_{kl} = \gamma/v_{kl}$. All these collision phases are stored in an adjacency matrix $\Gamma(t)$. The internal state of all particles at time $t = 0$ is initialized to $|+\rangle$. Then, the time-evolved state is again a weighted graph state given by (2), or (4) respectively. We study the entanglement that arises in such a system in the following.

One could compute entanglement properties by direct simulation of the Boltzmann gas. Here, however, we will focus on regimes where analytical results can be obtained, namely for large collision phases and arbitrary times, or for arbitrary phases in the limits of short and infinite times.

For further reference, we give here the relative velocity distribution. This can be easily obtained under the molecular chaos assumption by writing the velocity distribution of two gas particles—i.e., the product of two Maxwell–Boltzmann distributions (17)—in the centre of mass and relative coordinates and integrating out the centre of mass and the angular part of the relative velocity:

$$p_r(v) = 4\pi(4\pi\sigma^2)^{-3/2}v^2\exp[-v^2/(4\sigma^2)]. \tag{18}$$

4.1.1. Large collision phases. In a regime of large collision phases $\varphi \sim \gamma\sigma^{-1} \gg 1$ (i.e., large interaction constant or low temperatures) we can assign to each collision event a random phase in $[0, 2\pi]$. This already allows us to find the expected entropy for short times $rt < 1$, where $r = \pi d^2 n\langle v\rangle$ is the collision rate and $\langle v\rangle = \sqrt{16KT/(m\pi)}$ is the mean relative velocity. For short times, $rt < 1$, a particle will typically collide at most once (with probability rt). In such a collision the coherence of the single particle density matrix will decay as $\cos\varphi/2$, and hence the initially pure state $|+\rangle$ will become mixed state with eigenvalues $p = \cos^2(\varphi/4)$ and $1 - p = \sin^2(\varphi/4)$. The von Neumann entropy after such a collision is given by $S_\varphi(\rho_1) = H(p) = -p\log_2 p - (1-p)\log_2(1-p)$. The expected entropy of entanglement after a collision can be obtained by averaging over all possible collision phases:

$$\begin{aligned}
\langle S_1\rangle &= \frac{1}{2\pi}\int_0^{2\pi} S_\varphi(\rho_1)\,\mathrm{d}\varphi \\
&= -\frac{1}{\pi}\int_0^{2\pi}\mathrm{d}\varphi\cos^2(\varphi/4)\log_2[\cos^2(\varphi/4)] \\
&= -\frac{1}{\pi}\log_2(\mathrm{e})\left[\frac{\mathrm{d}}{\mathrm{d}x}\int_0^{2\pi}\mathrm{d}\varphi\cos^{2x}(\varphi/4)\right]_{x=1} \\
&= -2\log_2(\mathrm{e})\left[\frac{\mathrm{d}}{\mathrm{d}x}\frac{\Gamma[1/2+x]}{\Gamma[1/2]\Gamma[1+x]}\right]_{x=1} \\
&= -2\log_2(\mathrm{e})(1/2 - \ln(2)) = 2 - \log_2(e).
\end{aligned} \tag{19}$$

Taking into account that when no collision occurs (which happens with probability $1 - rt$) the state remains pure, and $S(\rho_1) = 0$, we find that the expected entropy of entanglement is $\langle S_1\rangle = rt(2 - \log_2 e) + \mathcal{O}[(rt)^2]$. The entropy of entanglement between a block A of size N_A

and the rest of the system B can be obtained by counting the average number of collisions that occur between particles of A and B:

$$\langle S_A\rangle \approx \frac{N_A N_B}{N-1} rt\,(2-\log_2 e) \qquad \text{for} \quad rt < 1. \tag{20}$$

For arbitrary times, we can obtain a lower bound to the von Neumann entropy using the following sequence of inequalities:

$$\begin{aligned}\langle S_A\rangle &\geqslant -\left\langle \log_2\left(\mathrm{tr}\rho_A^2\right)\right\rangle \geqslant -\log_2\left(\left\langle \mathrm{tr}\rho_A'^2\right\rangle\right)\\ &= -\log_2\left(\sum_{s_A,s'_A}\left\langle\left|C_{s_A,s'_A}\right|^2\right\rangle/2^{2N_A}\right).\end{aligned} \tag{21}$$

The first of these inequalities follows from a property of Réyni entropies as a measure of pure state entanglement. Rényi entropies, $S_R^q(\rho) = (1-q)^{-1}\log_2(\mathrm{tr}\,\rho^q)$, for $q > 0$ are known to be non-increasing functions of their parameter q, i.e., $S_R^q \leqslant S_R^{q'}$ for $q' > q$. Moreover, in the limit $q \to 1$ the Rényi entropy coincides with the von Neumann entropy, and therefore $S_R^2 = -\log_2(\mathrm{tr}\,\rho^2)$ provides a lower bound to the von Neumann entropy $S(\rho) = S_R^{q\to 1} \geqslant S_R^2$. From (9) we note that the coherence C_{s_A,s'_A} only depends on the difference $\boldsymbol{z}_A = \boldsymbol{s}_A - \boldsymbol{s}'_A$. In particular, the average $\left\langle\left|C_{s_A,s'_A}\right|^2\right\rangle$ depends only on the number Z_A of nonzero entries of $\boldsymbol{z}_A$:

$$\left\langle\left|C_{s_A s'_A}\right|^2\right\rangle = \prod_{k=1}^{N_B}\left\langle\cos^2\left(\tfrac{1}{2}\boldsymbol{z}_A\cdot\boldsymbol{\Gamma}_k\right)\right\rangle. \tag{22}$$

Each particle k in B will contribute with a factor $\int_0^{2\pi} \mathrm{d}\varphi\cos^2\varphi = 1/2$ to the product in (22) if it has collided with at least one particle of the subset of A where $\boldsymbol{z}_A$ has nonzero entries, whereas a factor 1 appears otherwise. Since in the regime under study collisions can be considered to be a Poissonian process, the probability that no such collision occurs is $p_{z_A} = \exp(-rtZ_A/N)$. Hence, each term in the product will contribute on average with a factor $1/2\left(1-p_{z_A}\right)+p_{z_A} = (1+\exp(-rtZ_A/N))/2$. Now, we only need to count the number of terms in the sum (21) that have a given number Z_A of nonzero entries in $\boldsymbol{z}_A$. A zero entry $z_A^i = 0$ occurs when the corresponding components of $\boldsymbol{s}_A$ and $\boldsymbol{s}'_A$ are equal $\left(s_A^i = s_A'^i\right)$, while a nonzero entry occurs when they are different $\left(s_A^i \neq s_A'^i\right)$. Since these two cases are equally probable, the number of terms, or vectors $\boldsymbol{z}_A$, with a given number of nonzero entries is given by the number of ways of ordering these nonzero entries, i.e., by the binomial factor $\binom{N_A}{Z_A}$. Putting these observations together we find

$$\langle S_A(t)\rangle \geqslant -\log_2\left(\frac{1}{2^N}\sum_{Z_A=0}^{N_A}\binom{N_A}{Z_A}\left(1+\mathrm{e}^{-rt\frac{Z_A}{N-1}}\right)^{N_B}\right). \tag{23}$$

This lower bound can be supplemented by the upper bound

$$\langle S_A\rangle \leqslant N_A\langle S_1\rangle. \tag{24}$$

The latter equation follows from the sub-additivity property of the von Neumann entropy.

Numerical results for $N_A \leqslant 8$ and arbitrary system sizes show that this lower bound is also a good estimate and describes well the behaviour of the entropic entanglement. Figure 9 shows the average entropy $\langle S_A\rangle$ of $N_A = 6$ particles in a background gas of 94 particles as a function of time together with the bounds (23) and (24).

In the short- or long-time limits we can simplify the above expression for the entanglement between two arbitrary parts of the Boltzmann gas. For short times $rtN_A/(N-1) < 1$, we

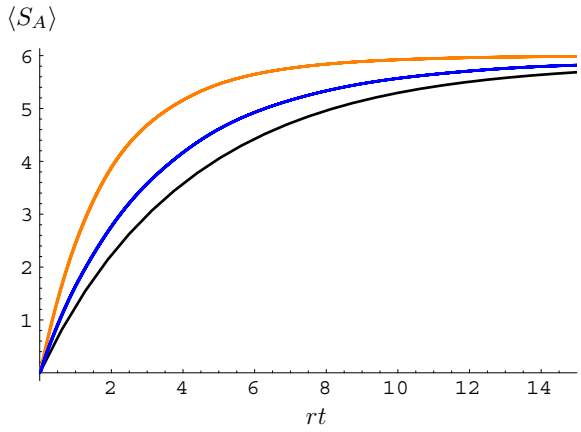

Figure 9. Average entanglement $\langle S_A\rangle$ of $N_A = 6$ particles in a background gas of $N_B = 94$ particles as a function of time rt (middle curve). Upper bound (upper curve) and lower bound (lower curve) are shown based on (23) and (24). Averages were taken over 100 simulation runs.

find

$$\langle S_A(t)\rangle \geqslant -\log_2\left(1-\frac{N_A N_B}{4(N-1)}rt\right) \approx \frac{N_A N_B}{4\ln 2(N-1)}rt,$$

which is consistent with the exact result (20) for short times.

4.1.2. Equilibrium state. In the long-time limit all particles will have collided with all other particles many times and accumulated phases $\varphi_{kl} \gg 1$, independently of the collision phase per collision. We refer to such a state as the *equilibrium* state. For sufficiently large times, $rt \gg N$, every term with $Z_A > 0$ in the sum (23) approaches one like the function $1 + N_B \exp[-rtZ_A/(N-1)]$ (disregarding the binomial factor), while the $Z_A = 0$ term is equal to two. One then finds

$$\begin{aligned}\langle S_A(t)\rangle &\geqslant -\log_2\left[\frac{2}{2^N}+\frac{1}{2^N}\sum_{Z_A=1}^{N_A}\binom{N_A}{Z_A}\left(1+N_B\,\mathrm{e}^{-\frac{rt}{N-1}Z_A}\right)\right]\\ &= -\log_2\left\{\frac{1}{2^N}\left[2+2^{N_A}-1+N_B\left(1+\mathrm{e}^{-\frac{rt}{N-1}}\right)^{N_A}-N_B\right]\right\}\\ &\approx -\log_2\left\{\frac{1}{2^N}\left[1+2^{N_A}+N_B\left(1+N_A\,\mathrm{e}^{-\frac{rt}{N-1}}\right)-N_B\right]\right\}\\ &= -\log_2\left(\frac{1}{2^{N_A}}+\frac{1}{2^{N_B}}-\frac{1}{2^N}+\tfrac{N_A N_B}{2^N}e^{\frac{-rt}{N-1}}\right).\end{aligned} \tag{25}$$

The equilibrium state ($rt \to \infty$) has thus the interesting feature that $|\Psi_\infty\rangle$ is maximally entangled with respect to *all* possible bipartitions, i.e., $S_A \approx N_A$, provided that the total number of particles N in the gas is sufficiently large. We would have expected such an asymptotic result by proposition 9 because the equilibrium states are random weighted graph states. These, when they are infinite, all have this property, and hence this is true also for the average entropy of entanglement. The result (25), on the other hand, is valid for finite N as well and is non-trivial especially in the case where both partitions are similarly large. In words, (25) says: for whatever bipartition one takes, the expected entropy of entanglement is

at most a single ebit away from its maximal value, $N_A \geqslant \langle S_A \rangle > N_A - 1$, and approaches N_A in the limit $N \to \infty$. For $N > 4$ it has been shown that strict maximal entanglement, i.e., $S_A = N_A$, cannot occur for all bipartitions of a pure state. However, we show that this limit can be achieved in an asymptotic sense, thus neither violating the statement for finite N nor proposition 9 valid for infinite N. The result is also in agreement with the findings of Page [44] and subsequent work [45] studying average or typical entanglement properties of the whole set of multipartite pure states.

Another remarkable property of the equilibrium state is that the localizable entanglement between *any* pair of particles approaches its maximum value of one e-bit as N increases. The proof is simple. For any pair of atoms $\{i, j\}$ with an interaction phase φ_{ij} we can find a third particle k with which both particles have accumulated a phase $\varphi_{ik} \approx \varphi_{jk} \approx \pi$. Then, imagine that we measure the remaining gas particles in the z-basis (to effectively decouple them) and particle k in the x-basis. A straightforward calculation shows that the resulting state of particles $\{i, j\}$ is always maximally entangled [8], no matter what the initial φ_{ij} was. Although the dynamics of the entanglement strongly depends on the particular type and regime of the semi-quantal gas, the equilibrium state will, in general, be of the form we just described. In particular, this equilibrium state also describes the semi-quantal Boltzmann gas in the regime of small collision phases, and the lattice gas studied below.

4.1.3. Small collision phases. To conclude our analysis of the semi-quantal Boltzmann gas, we consider the short-time entanglement in the regime of small collision phases. In this regime, we have to take into account the relative velocity of the colliding partners. A collision with relative velocity v will produce a decay of the coherence given by $|C_v|^2 = \cos^2[\varphi(v)/2]$. In addition, the probability that within a small time slot t a particle suffers a collision with relative velocity v is given by $p_c(v) = \pi d^2 v t n p_r(v)$. This can be easily seen in the reference frame of one of the particles: $p_c(v)$ is the volume swept by the moving particle during this time ($\pi d^2 v t$) times the probability to find such particle in that volume. The average decay is then given by

$$\begin{aligned}\langle |C_{01}|^2 \rangle_t &\approx \left(1 - \int \mathrm{d}v\; p_c(v)\right) + \int \mathrm{d}v\; p_c(v)|C_v|^2 \\ &= 1 - tn\pi d^2 \int \mathrm{d}v\; p_r(v) v (1 - |C_v|^2) = 1 - \alpha t. \end{aligned} \tag{26}$$

For small collision phases $\gamma\sigma^{-1} < 1$ the proportionality factor α can be approximated by

$$\alpha = 4\pi^2 d^2 n \left(\frac{1}{4\pi\sigma^2}\right)^{\frac{3}{2}} \int \mathrm{d}v\; v^3\, \mathrm{e}^{-\frac{v^2}{4\sigma^2}} \sin^2\left(\frac{\gamma}{2v}\right) \approx \frac{1}{4} n \sqrt{\pi} d^2 \frac{\gamma^2}{\sigma}.$$

Adding up all the contributions in (21) one immediately finds that the expected entanglement for one particle is $\langle S_1 \rangle \geqslant -\log_2(1 - \alpha/2)$. The expected entanglement of a block A of size N_A can be obtained by counting the collisions that occur between particles of A and the rest of the gas B.

$$\langle S_A(t) \rangle \geqslant -\frac{N_A N_B}{N-1} \log_2\left(1 - \frac{\alpha}{2} t\right) \approx \frac{\alpha}{2 \ln 2} \frac{N_A N_B}{N-1} t. \tag{27}$$

Thus, by writing $\alpha \approx \frac{1}{4}\sqrt{m\pi} d^2 \gamma^2 \frac{n}{\sqrt{k_B T}}$ we obtain the rate of entanglement generation in terms of the thermodynamical variables. Whereas in the regime of large collision phases entanglement grows with the rate of collisions ($\propto \sqrt{T}$), for small collision phases we find that entanglement generation is governed by the slow collision events (larger phases) leading to the opposite behaviour ($\alpha \propto \sqrt{T^{-1}}$).

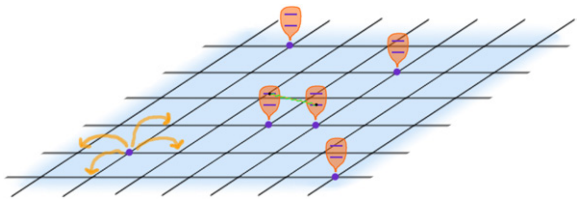

Figure 10. Illustration of a spin lattice gas. Particles can classically hop to neighbouring sites (arrows). Each particle carries internal spin degrees of freedom (here: two-level systems). Neighbouring spins can interact (symbolized by the line between them (centre)).

4.2. Lattice gas

In the previous subsection we concentrated on a dilute gas, such that correlations between particles did not depend on their mutual distance from each other at a certain time. Now, we study a lattice gas, where neighbourhood relations can play an important role. As before, we will start with all spins in the state $|+\rangle$ and use the interaction Hamiltonian (1) leading to weighted graph states. We will focus on the description in terms of the adjacency matrix Γ.

The quantum properties of the system are directly linked to the classical statistical properties of the gas through $\Gamma(t)$. In general, it is thus necessary to know the classical n-body distributions to give a complete description of the quantum state. Only for some gas models and regimes (like the Boltzmann gas presented above) correlations play a minor role and one can find analytical descriptions for single-particle phase-space distributions. In the remainder of this subsection, we study a lattice gas model that exhibits strong correlations. We use numerical simulations to recreate such classical correlations or, in other words, produce different realizations of $\Gamma(t)$ over which we later average. The model has the additional feature that it can possibly be implemented in a quantum optical system. It has already been demonstrated that an optical lattice can be used to store ultra-cold atomic gases. The degree of control in these experiments is extraordinary. Various system parameters can be adjusted—from the structure of the underlying periodic lattice to the interactions between the atoms—opening the door to a wide range of experiments and theoretical proposals [42, 46–52]. For a more exhaustive bibliography see the recent review [53]. In particular, one can choose a parameter regime where each lattice site is occupied by at most one atom [46, 49]. The internal quantum state of the atom (e.g. two meta-stable hyperfine states) can be stored in coherent superpositions over long time-scales (few minutes), while coherent inter-atomic interactions have also been achieved by cold collisions [47, 54]. These interactions correspond precisely to the Ising-type interactions chosen here. What is left to find are schemes to induce a random (incoherent) hopping of the atoms from one site to its neighbouring sites. We consider an $M \times M$ lattice containing N particles that randomly hop from site to site with a hopping rate η, and have nearest-neighbour interactions with coupling constant g_0 (see figure 10).

We use the above lattice gas model to investigate the typical multipartite entangled states that arise. An interesting observed effect is the creation of entangled clusters, that is, sets of particles that are connected in the graph, such that entanglement can be localized between any of the constituent particles. We find that the average number N_C of particles that form an entangled cluster grows exponentially with time. Similarly, the expected value for the maximal distance $\ell_{\max}$ between (localizable) entangled particles increases. After a finite time t_0, which only depends on the filling factor $\nu = NM^{-2}$ and the hopping rate η, almost all particles are connected. That is, after this time t_0, all particles are pairwise (localizable) entangled, and hence $\ell_{\max} \sim M$, suggesting a (bond) percolation phenomenon in the underlying graph.

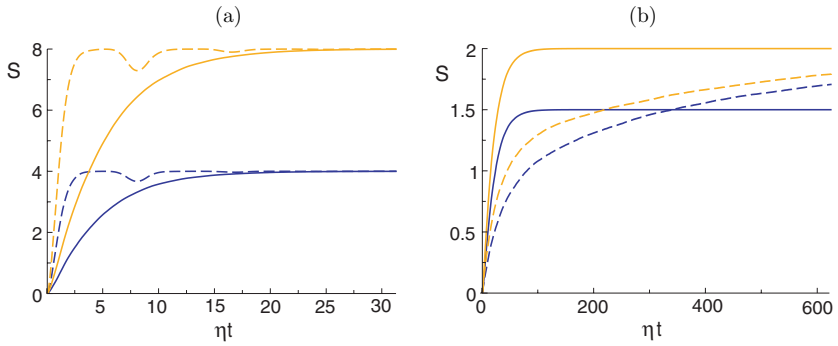

Figure 11. Lattice gas with $M = 20$, $g_0 = 0.8\eta$. (a) Average entropy of entanglement for block sizes $|A| = 4$ (dark) and $|A| = 8$ (light) and filling factors $\nu = 0.9$ (dashed) and $\nu = 0.25$ (solid). (b) Average entropy of entanglement for two probe particles that are initially located at a relative distance $\ell = 0$ (dark) and $\ell = 8$ (light) and have hopping rates $\eta_p = 0$ (solid) and $\eta_p = \frac{1}{5}\eta$ (dashed).

Concerning block-wise entanglement, figure 11 shows the expected entanglement between a set of randomly chosen particles and the rest of the system as a function of time. Since all the density matrix elements are initially equal because $|+\rangle^{\otimes N}$ is the initial state, and since all coherences decay to zero with time, we find that the entanglement saturates to its maximum value. At high filling factors the entropy of entanglement undergoes periodic decreases every time the typical accumulated phase $\varphi_{1k}(t)$ with a nearest neighbour reaches 2π, i.e., at $t \approx k2\pi/g$ with integer k. At lower filling factors we can observe that the entanglement is not additive when increasing the block-size, which indicates the presence of correlated collisions. To highlight this effect, we consider the case where two probe particles move freely in the lattice—with a hopping rate η_p possibly different from the hopping rate of the background particles—and only interact with the gas particles that are in the same position[5].

Figure 11(b) shows the entanglement of the probes with the rest of the system for different initial relative distances ℓ between the two probes, and for different probe hopping rates η_p. Small probe hopping rates favour repeated collisions with the same particle as opposed to independent collisions with different particles. This amounts to coherent addition of the interaction phase, which leads to a much higher rate of entanglement generation because coherences decay faster (for $k\delta\varphi < 1$, $\cos(k\delta\varphi/2) \leqslant \cos(\delta\varphi/2)^k$). At $\ell = 0$ and fixed probes ($\eta_p = 0$), all the collisions with gas particles are exactly correlated. Under these circumstances the coherences of the type $\rho_{01,10}$ remain untouched (see subsection 5.2) while all others decay to zero, leading to a maximal entropy of $S(\infty) = 1.5$. When the probe particles are given a nonzero hopping rate, they start to undergo independent collision events which eventually turn the reduced density matrix into a completely mixed one ($S = 2$).

This suggests that classical correlations in the collisions, e.g. induced by the geometry of the set-up, can significantly influence the entanglement properties of the system. Indeed, we find such correlation effects also in the context of decoherence processes of certain entangled probe states, e.g. if we vary the distance of the probe particles [8]. Short distances mainly allow for correlated collisions, whereas with increasing distance uncorrelated collisions are favoured. We turn to these phenomena in the following section.

[5] A possible implementation could consist of three different layers of a 3D optical lattice: the middle layer for the gas, sandwiched between the layers where each of the probes moves independently. We can choose probes of a different species to selectively change their hopping rate.

5. Decoherence in spin systems

Decoherence is a fundamental mechanism believed to be responsible for the transition from the quantum to the classical world [55]. Interactions between system degrees of freedom and environment degrees of freedom lead to entanglement, manifesting itself in the decoherence of the system state. Many decoherence models have been discussed in the literature, most prominent among them oscillator bath models [56] and spin bath models [57]. Here, we study a physically motivated model of a mesoscopic inhomogeneous spin bath. In particular, we describe the environment by a *spin gas* [8]. This model has the advantage that it can be described in the framework of weighted graph states, thus allowing us to treat the entire spin bath without approximations.

We remark that the same methods could be used to study decoherence phenomena in spin chains and lattices of the same type as in section 3. If subset A of spins is considered as the system, and the rest B as the bath then tracing out all particles in B leads to similar decoherence effects, although the structure and order we have in the lattice and hence in the subset B are somewhat in contrast to the usual idea of a bath. Still, since e.g. the production of cluster states for one-way quantum communication will in practice never be perfect, one is naturally led to weighted graph states and to the question how the 'pollution' of the cluster state by unwanted weighted graph connections influences the one-way quantum computations. Here, however we derive the following results:

- a spin gas has memory, i.e., induces non-Markovian decoherence;
- explicit decoherence maps (single qubit);
- multipartite decoherence maps and stability of probe states
- finite size effects.

We analyse a microscopic decoherence model in which the environment is described as a spin gas. For various multipartite entangled probe states, we analyse the decoherence induced by interactions between the probe- and environmental spins in such spin gases. Throughout the section, we concentrate on a specific realization of a spin gas, the spin lattice gas, and show the effects of non-Markovian and correlated noise, as well as finite size effects. However, our methods can be easily applied to decoherence in other spin gases, such as a Boltzmann gas.

The probe system A consists of N_A qubits prepared in some arbitrary state. In principle, we could include some system Hamiltonian H_A without having to change the methods developed in the previous sections, but we will concentrate on the situation $H_A = 0$ and merely consider the decoherence that the initial, arbitrary state suffers due to the environment. The system qubits interact with the uncontrollable degrees of freedom of this environment, the lattice gas B, via the interaction Hamiltonian (1). Observe that the environment spins can themselves interact among each other by the same interaction Hamiltonian, and this does not influence the system A. One can even choose a different Hamiltonian for interactions within the environment. For all the results in this subsection to hold, the only requirement is that the diagonal elements of the environment's state—in the canonical basis—remain unchanged. This means that in a possible physical realization of such decoherence studies one can relax the experimental conditions that would be necessary to keep the background gas in a coherent state. Initially we assume that the environment is not correlated with the system, as is often done in system-bath studies, and further that the environment is in the product state $|+\rangle^{\otimes N_B}$, which is, after what we just said about interactions within the system B, not a strong restriction.

We now proceed to study the explicit time dependence of the map for a single qubit, where we concentrate on one central aspect: Markovian versus non-Markovian dynamics.

5.1. Decoherence of a single qubit

We derive the time-dependent decoherence map corresponding to a particular collision history for a single qubit in a spin gas using the PEPs picture for maps developed in subsection 2.3.4. Here, the subsystem is $A = \{1\}$, so the interaction phases with the other qubits l are φ_{1l}. We have $|\Phi\rangle = |\varphi^+\rangle$ and the expression for $E_t^{(l)}$ simplifies to $E_t^{(l)} = (|\varphi^+\rangle\langle\varphi^+| + |\chi_1\rangle\langle\chi_1|)$ with $|\chi_1\rangle_{1'1} = 1/\sqrt{2}(|00\rangle_{1'1} + \mathrm{e}^{\mathrm{i}\varphi_{1l}}|11\rangle_{1'1})$. We omit normalization (since in the PEPs picture we have to normalize the final state anyway), then $E_t^{(l)}$ has the matrix form in the computational basis:

$$E_t^{(l)} \propto \begin{pmatrix} 1 & 0 & 0 & 1/2(1+\mathrm{e}^{-\mathrm{i}\varphi_{1l}}) \\ 0 & 0 & 0 & 0 \\ 0 & 0 & 0 & 0 \\ 1/2(1+\mathrm{e}^{\mathrm{i}\varphi_{1l}}) & 0 & 0 & 1 \end{pmatrix}.$$

We obtain E_t by Hadamard multiplication of all $E_t^{(l)}$ and a final normalization, which is $1/2$ in this case. Using $1/2(1+\mathrm{e}^{\pm\mathrm{i}\varphi}) = \cos(\varphi/2)\,\mathrm{e}^{\pm\mathrm{i}\varphi/2}$ and defining $r := \prod_l \cos(\varphi_{1l}/2)$, $\gamma := \sum_l \varphi_{1l}/2$, the two nonzero off-diagonal elements of E_t can be written as $r\mathrm{e}^{\pm i\gamma}$. The coefficients of the map in the Pauli basis are computed as $\lambda_{k_1 l_1} = \langle\phi_{k_1}|E_t|\phi_{l_1}\rangle$ with $k_1, l_1 \in \{0,1,2,3\}$ and $|\phi_{k_1}\rangle = \mathbb{1}_{1'} \otimes (\sigma_{k_1})_1|\varphi^+\rangle$. As nonzero coefficients we get $\lambda_{00} = (1 + r\cos\gamma)/2$, $\lambda_{33} = (1 - r\cos\gamma)/2$, and $\lambda_{03} = \lambda_{30}^* = (\mathrm{i}r\sin\gamma)/2$, so the map reads

$$\mathcal{E}_t\rho = \lambda_{00}\rho + \lambda_{33}\sigma_z\rho\sigma_z + \lambda_{03}(\mathbb{1}\rho\sigma_z - \sigma_z\rho\mathbb{1}). \tag{28}$$

Let us point out that this map corresponds to a particular collision history at time t, i.e., for given values of the $\varphi_{1l}(t)$. The explicit time dependence of the map depends crucially on how this collision phases evolve. Depending on the parameter regime, semi-quantal gases can follow various collision patterns and display Markovian or non-Markovian features. Both effects can already be seen in the evolution of a single probe particle, and essentially correspond to the following two types of collision patterns that occur during a short time interval Δt:

(i) Markovian: at every time step δt the probe particle collides with a different particle and accumulates a small interaction phase $\delta\varphi$. The state of the probe particle will then decohere exponentially fast with the number of time steps $k = \Delta t/\delta t$:

$$|\rho_{01}| = [\cos(\delta\varphi/2)]^k = \mathrm{e}^{-\Delta t/\tau_e}$$

with $\tau_e \approx 8\delta t/\delta\varphi^2$.

(ii) Non-Markovian (or coherent coupling): in the time interval Δt a given gas particle has collided k times with the probe. The coherent addition of the interaction phase leads to a Gaussian type of decay:

$$|\rho_{01}| = \cos(k\delta\varphi/2) \approx \mathrm{e}^{-\Delta t^2/(2\tau_g^2)}$$

with $\tau_g = 2\delta t/\delta\varphi$.

To get a proper decoherence map, it is not enough to trace out the quantum degrees of freedom of the environment. We have to take into account that we do not control the classical degrees of freedom of the background gas, i.e., we should average the effect of the maps $\mathcal{E}_t(\rho)$ over all collision patterns that might have occurred up to the given time. This can be conveniently written as $\bar{\mathcal{E}}_t(\rho) = \bar{C} \circ \rho$ with

$$\bar{C}_{s,s'}(t) = \int \mathrm{d}\,\Gamma p_t(\Gamma) C_{s,s'}(\Gamma),$$

where $p_t(\Gamma)$ is the probability that at a time t the adjacency matrix is Γ. So, the phase factor in (8) suffers two types of averaging effects, one over collision histories, and the other one

over all possible combinations of excited (i.e., state $|1\rangle$) collision partners, i.e., over all $\boldsymbol{s}_B$:

$$\bar{C}_{s,s'}(t) = \frac{1}{2^{N_B}} \sum_{\boldsymbol{s}_B} \int \mathrm{d}\Gamma \; p_t(\Gamma)\, \mathrm{e}^{\mathrm{i}(\boldsymbol{s}-\boldsymbol{s}')\cdot\Gamma\cdot\boldsymbol{s}_B} = \int \mathrm{d}\epsilon p_{\boldsymbol{z}}(\epsilon)\, \mathrm{e}^{\mathrm{i}\epsilon}, \tag{29}$$

where we see that a complete characterization of the dynamics of the probe can be given in terms of the overall probability distribution $p_{\boldsymbol{z}}(\epsilon)$. Here, $\epsilon = \boldsymbol{z}\cdot\Gamma_{AB}\cdot\boldsymbol{s}_B$ is the overall phase for a given coherence specified by the binary vector $\boldsymbol{z} = \boldsymbol{s} - \boldsymbol{s}'$. One then finds that the coherence falls off essentially with the width $\sigma_\Gamma(t)$ of the distribution as $\exp(-\sigma_\Gamma(t)^2/2)$ and acquires a phase $\Phi \sim \langle\epsilon\rangle$. The two extreme regimes mentioned before correspond to $\sigma_\Gamma(t) \propto \sqrt{t}$ (Markovian) and $\sigma_\Gamma(t) \propto t$ (non-Markovian). We point out that the dynamics will typically be very rich showing combinations of both effects and further non-trivial features such as finite-size effects.

When calculating average locally invariant quantities, such as the expected entanglement, we argued that the phase factor multiplying the product of cosines in the coherences (9) could be neglected since they could be cancelled by the local operation (13). When calculating such properties on decohered states these factors cannot be neglected since, in principle, we have no control over the collision phases and hence cannot produce the corresponding local unitary. The presence of this phase factor will induce an additional decoherence with respect to the case where it is not present (see section 5.3).

5.2. Decoherence of entangled two-qubit states

Besides of the signatures of Markovian/non-Markovian dynamics studied in the single-qubit case, the case of two (or more) probe qubits exhibits the feature of correlated versus uncorrelated decoherence processes. We say that an uncorrelated decoherence process occurs when both probe particles interact with different environment particles, while a completely correlated decoherence process is given when both probe particles interact with the same environment particle *and* pick up the same interaction phase. Without the last condition, the process is partly correlated as it can be split up into a correlated and an uncorrelated part.

The typical situation in a spin gas is the following. Assume one of the probe particles has interacted with an environment particle that had not yet interacted with either of the two probe particles (a fresh particle). Then, this event will affect the momentary density matrix of the two probe particles as an uncorrelated decoherence process. If, at a later time, the other probe particle interacts with the same environment particle, then the process is turned into a (partly) correlated decoherence process since the spin gas remembers its interaction history. In this situation correlated decoherence processes are a consequence of the non-Markovian property of spin gases.

However, correlated decoherence processes can also exist independently of the non-Markovian property. Assume that the probe particles are held close together (so they are not really part of the spin gas that surrounds them). Then, even if they always meet fresh particles, which corresponds to a transition to a Markovian spin gas, there are correlated decoherence processes when the probes interact with the fresh particles almost at the same time.

In the following we first give a simple, analytical example showing how different coherences react differently to correlated and uncorrelated collision events. Here, coherences are off-diagonal elements in a reduced density matrix represented in the computational basis. Since the coherences are affected differently this implies that some states are more robust against correlated decoherence processes compared to uncorrelated ones, while the situation is reversed for others. Subsequently, we will highlight the two different effects (non-Markovian

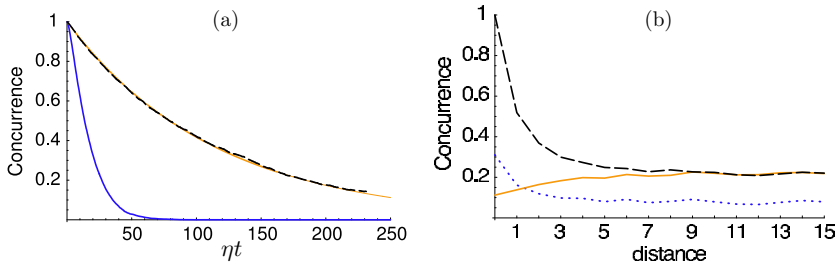

Figure 12. (a) Concurrence of two probe particles prepared in a maximally entangled Bell state $|\varphi^+\rangle \propto |00\rangle + |11\rangle$ in a 100×3200 lattice gas with $N = 8 \times 10^4$ for $g_0 = 0.8\eta$ and fixed probes (solid); and fast moving probes (dashed). The solid, light curve corresponds to an analytical result obtained in a Markovian regime. (b) Concurrence of two probe particles at time $t_1 = 25\eta^{-1}$ for different initial entangled states as a function of distance d between the probes : $|\psi^+\rangle \propto |01\rangle + |10\rangle$ (dashed-dark), $|\varphi^+\rangle$ (solid-light), and $|G\rangle \propto |{+}0\rangle + |{-}1\rangle$ (dotted).

versus Markovian and correlated versus uncorrelated) with numerical simulations in a lattice gas.

As in the case of one qubit one can derive the decoherence map in the Pauli basis using the PEPs picture. The expression one obtains is rather lengthy. So we study the features of this map in terms of the coherences C_{s_A,s'_A} in the framework of subsection 2.3.3. The following example demonstrates the difference between correlated and uncorrelated decoherence processes.

From (9) we find that if a part $A1$ of the probe subsystem A does not have any common collision partners with the rest $A2$ of the subsystem then $C_{s_A,s'_A} = C_{s_{A1},s'_{A1}} C_{s_{A2},s'_{A2}}$ where $\boldsymbol{s}_A = (\boldsymbol{s}_{A1}, \boldsymbol{s}_{A2})$. Accordingly, we will say that the maps or channels acting on each part of the sub-system are *independent* (or uncorrelated)[6]. On the other hand, if two parts of the subsystem share collision partners then some coherences will be nearly unaffected by such correlated collisions, while others will suffer an increased decay (as compared to uncorrelated collisions). For instance, consider the case where two probe particles (1 and 2) have a very similar collision pattern, i.e., $\Gamma_{2j} = \Gamma_{1j} + \delta_j$ for all j, then it follows that coherences associated with $|01\rangle\langle 10|$ will only decay by a factor $2^{-N_B} \sum_{s_B} \mathrm{e}^{\mathrm{i}\boldsymbol{\delta}\cdot\boldsymbol{s}_B}$, while $|11\rangle\langle 00|$ will be 'super-damped' by $2^{-N_B} \sum_{s_B} \mathrm{e}^{\mathrm{i}(2\Gamma_1+\boldsymbol{\delta})\cdot\boldsymbol{s}_B}$.

We now study the decoherence of different, initially entangled two-qubit states by numerical simulations. In order to explore different regimes, we imagine a scenario where the probe particles can be displaced at a constant speed v relative to the gas. By varying the speed v and the distance d between the probe particles, we can highlight two effects.

- By decreasing the probe speed, we analyse the effect of multiple interactions with the same particle in contrast to interactions with different (independent) particles.
- By increasing the distance, we turn from correlated to uncorrelated collisions between probe and environment particles.

For two qubits, the concurrence [58] is an entanglement measure, defined as $C(\rho) := \max\{0, \lambda_0 - \lambda_1 - \lambda_2 - \lambda_3\}$, where the λ_i are the eigenvalues of the matrix $\rho\tilde{\rho}$ in decreasing order, and $\tilde{\rho} := (\sigma_y \otimes \sigma_y)\rho^*(\sigma_y \otimes \sigma_y)$ with the complex conjugation taken in the standard basis. Figure 12(a) shows the decay of entanglement, as measured by the concurrence, of an initial Bell state $|\varphi^+\rangle \propto |00\rangle + |11\rangle$ in two extreme scenarios: (i) fixed probe particles ($v = 0$).

[6] However, there might actually be small correlations between the channels because the presence of a particle in the neighbourhood of a probe particle might change the probabilities for a second particle to collide in a different part of the subsystem.

(ii) Large probe speeds, $v/a \gg \eta$, where a is the inter-site spacing. A fixed value $\varphi = 0.1$ is assigned to the collision phase every time a probe particle crosses an occupied site. These two scenarios illustrate the difference between Markovian and non-Markovian environments. A large probe speed enforces a perfectly Markovian behaviour. One can see this in the following way. At every time step, each probe particle interacts with a new environment particle with probability ν. Hence, after a number s of time steps, the relevant coherence is given by $|C_{00,11}| = |C_{0,1}|^2 = |\nu \exp(\mathrm{i}\delta_\varphi/2)\cos(\delta_\varphi/2) + (1-\nu)|^{2s}$. The numerical data match the analytical curve derived in this way. Figure 12(b) shows the concurrence at a given time t_1 as a function of the distance for three different entangled states: two Bell states and a cluster state (see figure caption). For Bell states the concurrence is equal to the absolute value of their only nonzero off-diagonal element in the density matrix, and therefore figure 12 provides direct information about the individual coherences. The figure shows the influence of correlated collisions: coherences $\rho_{01,10}$ (in $|\psi^+\rangle$) are robust against correlated noise, and coherences $\rho_{00,11}$ (in $|\varphi^+\rangle$) are especially fragile under correlated noise. The remaining coherences decay in the same way under correlated or uncorrelated noise (hence, the weak distance dependence of $|G\rangle$). From figure 12(b) we also see that the immediate environments of each probe become more independent as d increases.

The above results show that classical correlations in the collisions, e.g. induced by the geometry of the set-up, can significantly influence the entanglement properties of the system.

5.3. Decoherence of multipartite entangled states

We now apply our method to investigate the decoherence of different multipartite entangled probe states of N_A qubits. Due to the lack of simple, computable multipartite entanglement measures, we use the negativity of bipartitions [59] as an indicator of multipartite entanglement in the system. That means, we consider bipartitions of the system, i.e., a partition consisting of a set of particles A_k and its complement $\bar{A}_k$, and investigate the entanglement properties with respect to the $2^{N_A-1}-1$ independent bipartitions [60, 61]. In general, we get a broad picture of multipartite entanglement in this way. For each bipartition we can determine its negativity $\mathcal{N}_{A_k} = (||\rho^{T_{A_k}}||_1 - 1)/2$ [59, 62]. We define two multipartite entanglement measures:
(i) the *average negativity* $\bar{\mathcal{N}}$, as the average over all bipartitions,

$$\bar{\mathcal{N}} = 1/(2^{(N_A-1)} - 1)\sum_{A_k} \mathcal{N}_{A_k},$$

and (ii) the minimal negativity

$$\mathcal{N}_{\min} = \min\{\mathcal{N}_{A_k}\}.$$

Zero average negativity is a necessary condition for full separability of the state, and $\mathcal{N}_{\min} = 0$ is a sufficient condition that the state is not multi-party distillably entangled.

We examine different multipartite entangled probe states that interact with a lattice gas through a pairwise Ising Hamiltonian $H_{kl} = \sigma_z^{(k)} \otimes \sigma_z^{(l)}$. The evolution under the Ising Hamiltonian has very similar properties compared to the evolution under the locally unitarily equivalent Hamiltonian $H_{kl} = |11\rangle_{kl}\langle 11|$, and hence most of the previous conclusions will apply. We choose the Ising Hamiltonian here for convenience because coherences are still scaled in essentially the same way but do not include a phase factor:

$$C_{s_A s'_A} = \prod_{k=1}^{N_B} \cos[(\boldsymbol{s}_A - \boldsymbol{s}'_A)\cdot \boldsymbol{\Gamma}_k]. \tag{30}$$

The probe states under consideration will be (linear) cluster states $|\chi\rangle$ [15, 16], GHZ-states and W-states

$$|W\rangle \propto \sum_{i=1}^{N_A} |w_i\rangle,$$

where $|w_i\rangle$ is the state corresponding to all spins in state zero except the ith that is in one. Since the noise process is basis dependent, we study variants of GHZ states corresponding to different local bases:

$$|\Psi\rangle \propto |0\rangle^{\otimes N_A} + |1\rangle^{\otimes N_A}$$
$$|\Psi'\rangle \propto |0\rangle|+\rangle^{\otimes N_A-1} + |1\rangle|-\rangle^{\otimes N_A-1}$$
$$|\Psi''\rangle \propto |+\rangle|0\rangle^{\otimes N_A-1} + |-\rangle|1\rangle^{\otimes N_A-1}.$$

The decay of the average negativity is plotted in figure 14(a). To qualitatively understand the different behaviour of the curves we derive analytic results in the limit of independent environments for each particle $k \in A$ (only uncorrelated collision events). In this limit, the decoherence process can be described by a tensor product of single-qubit dephasing maps:

$$\mathcal{E}_t^{(k)}\rho = p_k\rho + (1-p_k)\sigma_z^{(k)}\rho\sigma_z^{(k)}, \qquad \text{where} \quad p_k = \frac{1}{2}\left(1 + \prod_{l\in B}\cos(2\varphi_{kl}(t))\right). \tag{31}$$

These single-qubit maps can be derived similarly as in subsection 5.1, where the only difference is that we use an Ising–Hamiltonian now. Still, a PEPs picture as in subsection 2.3.4 remains valid, such that every single-qubit map can be computed with the Hadamard product trick. Coherences in these single-qubit density matrices decay as $\rho_{01}^{(k)}(t) = (2p_k - 1)\rho_{01}(0)$. As before, the precise time dependence of decoherence will be given by the average $\bar{p}_k(t) = \langle p_k\rangle_{\Gamma(t)}$ over different realizations. We assume that this average value is the same for every probe particle k, i.e., $\bar{p}_k =: p$ for all k. Note that the formulae below retain the same form if no average over interaction histories is taken and p is assumed to represent only one particular interaction history.

The average negativities for the three GHZ states given above are

$$\bar{\mathcal{N}}(|\Psi\rangle) = \frac{1}{2}|2p-1|^{N_A},$$

$$\bar{\mathcal{N}}'(|\Psi'\rangle) = -\frac{1}{2}\left[1 - \frac{1}{2^{N_A-1}-1}\sum_{b=1}^{N_A-1}\binom{N_A-1}{b}\sum_{k=0}^{N_A-1}p^{N_A-1-k}(1-p)^k \right.$$
$$\left. \times \sum_{l=\max\{0,k-N_A+1+b\}}^{\min\{k,b\}}\binom{b}{l}\binom{N_A-1-b}{k-l}\max\{1,(2p-1)p^{2l-b}(1-p)^{b-2l}\}\right],$$

$$\bar{\mathcal{N}}''(|\Psi''\rangle) = \frac{1}{2^{N_A-1}-1}\left[\mathcal{N}''_{\min} + (2^{N_A-1}-2)\frac{1}{2}|2p-1|^{N_A-1}\right] \qquad \text{with}$$
$$\mathcal{N}''_{\min} = \frac{1}{4}\max\{0, |2p-1| + |2p-1|^{N_A-1} + |2p-1|^{N_A} - 1\}. \tag{32}$$

For W-states, we obtain $\mathcal{N}^W_{\min} = \sqrt{(N_A-1)}/N_A \approx 1/\sqrt{N_A}$ and

$$\bar{\mathcal{N}}^W = \frac{|2p-1|^2}{N_A(2^{N_A}-2)}\sum_{b=1}^{N_A-1}\binom{N_A}{b}\sqrt{b(N_A-b)}. \tag{33}$$

Proof.

(i) *GHZ-state* $|\Psi\rangle$. From (31) we have

$$\bigotimes_k \mathcal{E}_t^{(k)}(|\Psi\rangle\langle\Psi|) = 1/2\Bigg(|0\rangle^{\otimes N}\langle 0|^{\otimes N} + \prod_{j=1}^{N}(2p_j-1)|0\rangle^{\otimes N}\langle 1|^{\otimes N} + \prod_{j=1}^{N}(2p_j-1)|1\rangle^{\otimes N}\langle 0|^{\otimes N} + |1\rangle^{\otimes N}\langle 1|^{\otimes N}\Bigg)$$

in the computational basis. Every partial transposition moves the two off-diagonal elements along the anti-diagonal. The eigenvalues of all partial transpositions are hence the same, especially there is only one negative eigenvalue $\lambda = -\left|\prod_{j=1}^{N}(2p_j-1)\right|$. The negativities for all partial transpositions are $N_{A_k} = \prod_{j=1}^{N}|2p_j-1|$, so $\bar{N} = N_{A_k}$. If $p_j = p$ for all $j \in \{1,\ldots,N\}$, then $\bar{N} = \frac{1}{2}|2p-1|^{N_A}$ as claimed.

(ii) $|\Psi''\rangle = 1/2(|+\rangle_1|0,\ldots,0\rangle_{2,\ldots,N} + |-\rangle_1|1,\ldots,1\rangle_{2,\ldots,N})$. Compared to the GHZ state $|\Psi\rangle$ only the first qubit has been changed by a local Hadamard transformation. Hence, there are only two types of partial transpositions. First, there are $2^{N_A}-2$ partial transpositions, which all have the same negativity $\prod_{j=2}^{N}|2p_j-1|$ by the same reasoning as in (i). Only the partial transposition of qubit 1 alone is different. When we apply $\otimes_k \mathcal{E}_t^{(k)}$ to $\left|\Psi''\right\rangle\langle\Psi''|$, express the density matrix in the computational basis and relabel matrix rows and columns, then all nonzero matrix entries are in a 2-qubit subspace. With $c_1 := (2p_1-1)$ and $c_r := \prod_{j=2}^{N}(2p_j-1)$ this matrix is

$$\bigotimes_k \mathcal{E}_t^{(k)}(|\Psi''\rangle\langle\Psi''|) = 1/4\begin{pmatrix} 1 & c_r & c_1 & -c_1c_r & \mathbf{0} \\ c_r & 1 & c_1c_r & -c_1 & \\ c_1 & c_1c_r & 1 & -c_r & \\ -c_1c_r & -c_1 & -c_r & 1 & \\ \mathbf{0} & & & & \mathbf{0} \end{pmatrix}.$$

The nonzero eigenvalues are $1/4(1-c_r-c_1-c_1c_r)$, $1/4(1-c_r+c_1+c_1c_r)$, $1/4(1+c_r-c_1+c_1c_r)$, $1/4(1+c_r+c_1-c_1c_r)$, of which only one can be negative depending on the signs of c_r and c_1. Putting absolute values the four cases can be expressed in a single equation, $\lambda = -1/4(1-|c_r|-|c_1|-|c_1||c_r|)$. If all p_j are the same, we have the negativity $\mathcal{N}''_{\min} := \mathcal{N}''_{\{1\}} = \frac{1}{4}\max\{0, |2p-1| + |2p-1|^{N_A-1} + |2p-1|^{N_A} - 1\}$. Combining this result with the negativity of the other partial transpositions using the appropriate weight leads to the final expression for $\mathcal{N}''$.

(iii) *Graph-GHZ state* $|\Psi'\rangle$. We use the following notation. If $a \in \{0,1\}$ then $\bar{a} = \mathrm{not}(a) = a \oplus 1$, where the symbol $\oplus$ means addition modulo 2. If $\boldsymbol{a}$ is a binary vector, then $\bar{\boldsymbol{a}} = \mathrm{not}(\boldsymbol{a}) = \boldsymbol{a} \oplus (1,\ldots,1)$. Further, in this proof, $|\boldsymbol{a}| := \|\boldsymbol{a}\|_1 = \sum_k a_k$ and $|\bar{\boldsymbol{a}}| = n - |\boldsymbol{a}|$ if $\boldsymbol{a}$ has length n. We define the graph state basis for an N_A-qubit graph-GHZ state with $\boldsymbol{a}$ being an N_A-binary vector as $|\Psi_{\boldsymbol{a}}\rangle := \otimes_{k=1}^{N_A}\left(\sigma_z^k\right)^{a_k}|\Psi_{\mathbf{0}}\rangle$, where $|\Psi_{\mathbf{0}}\rangle = |\Psi'\rangle$ and $a_k \in \{0,1\}$ are the components of $\boldsymbol{a}$. When assume that all p_k are the same in (31) then

$$\bigotimes_k \mathcal{E}_t^{(k)}(|\Psi_{\mathbf{0}}\rangle\langle\Psi_{\mathbf{0}}|) = \sum_{\boldsymbol{a}} p^{N_A-|\boldsymbol{a}|}(1-p)^{|\boldsymbol{a}|}\,|\Psi_{\boldsymbol{a}}\rangle\langle\Psi_{\boldsymbol{a}}|\,.$$

When we write this graph-diagonal state in the product basis $\{|0\rangle|+\cdots+\rangle, \ldots, |0\rangle|-\cdots-\rangle, |1\rangle|+\cdots+\rangle, \ldots, |1\rangle|-\cdots-\rangle\}$ it has the following structure:

$$\begin{pmatrix} d_1 & & & & \tilde{d}_1 \\ & d_2 & & \tilde{d}_2 & \\ & & \cdots & & \\ & \tilde{d}_2 & & d_2 & \\ \tilde{d}_1 & & & & d_1 \end{pmatrix}.$$

The characteristic function can e.g. be computed by a recursion formula, which is obtained through expansion of the determinant into sub-determinants. The eigenvalues are $\lambda_j^{\pm} = d_j \pm \tilde{d_j}$. We relabel all '+' as '0' and all '−' as '1' in the above product basis, then we can use binary notation again. Let $\boldsymbol{K}$ be an N_A-binary vector of the form $(0, \boldsymbol{k})$, where $\boldsymbol{k}$ is an $(N_A - 1)$-binary vector, then the diagonal elements (corresponding to the ds above) are

$$c_{\boldsymbol{K},\boldsymbol{K}} = c_{\bar{\boldsymbol{K}},\bar{\boldsymbol{K}}} = \tfrac{1}{2} p^{N_A-1-|\boldsymbol{k}|}(1-p)^{|\boldsymbol{k}|},$$

and the anti-diagonal elements (corresponding to the $\tilde{d}$s above) are

$$c_{\boldsymbol{K},\bar{\boldsymbol{K}}} = c_{\bar{\boldsymbol{K}},\boldsymbol{K}} = \tfrac{1}{2}(2p-1) p^{N_A-1-|\boldsymbol{k}|}(1-p)^{|\boldsymbol{k}|}.$$

Any partial transposition simply permutes the elements on the anti-diagonal. Choose a bipartition $B - \bar{B}$ of the N_A qubits. Let $\boldsymbol{B}$ be an N_A-binary vector of the form $(0, \boldsymbol{b})$, where $\boldsymbol{b}$ is an $(N_A - 1)$-binary vector, which has ones in the places j if qubits j belong to B, and zeros otherwise. The eigenvalues of ρ^{T_B} with respect to the partial transpose T_B can now be written in binary notation as

$$\lambda_{\boldsymbol{k}}^{\pm} = c_{\boldsymbol{K},\boldsymbol{K}} \pm c_{\boldsymbol{K}\oplus\boldsymbol{B},\bar{\boldsymbol{K}}\oplus\boldsymbol{B}} = \tfrac{1}{2} p^{N_A-1-|\boldsymbol{k}|}(1-p)^{|\boldsymbol{k}|} \pm \tfrac{1}{2}(2p-1) p^{N_A-1-|\boldsymbol{k}\oplus\boldsymbol{b}|}(1-p)^{|\boldsymbol{k}\oplus\boldsymbol{b}|}.$$

Through relabelling we can always bring $\boldsymbol{B}$ to the form $(0, 1, \ldots, 1, 0, \ldots, 0)$, where there are $b := |\boldsymbol{B}| = |\boldsymbol{b}| = \mathrm{card}(B)$ ones. Observe that there are $\binom{N_A-1}{b}$ bipartitions which map to this vector and have the same eigenvalues of the partially transposed density matrix. With $\boldsymbol{B}$ in this special form, we have $|\boldsymbol{k} \oplus \boldsymbol{b}| = |(\bar{k}_1, \bar{k}_2, \ldots, \bar{k}_b, k_{b+1}, \ldots, k_{N_A-1})|$. We set $k := |\boldsymbol{k}|$. If there are l ones in $(k_1, \ldots, k_b)$ then there are $k - l$ ones in $(k_{b+1}, \ldots, k_{N_A-1})$ and $b - l$ ones in $(\bar{k}_1, \ldots, \bar{k}_b)$, so there are $|\boldsymbol{k} \oplus \boldsymbol{b}| = k + b - 2l$. Furthermore, the number of ways to arrange l ones in $(k_1, \ldots, k_b)$ and $k-l$ ones in $(k_{b+1}, \ldots, k_{N_A-1})$ is $\binom{b}{l}\binom{N_A-1-b}{k-l}$. The following constraints hold. (1) $l \leqslant k$, (2) $l \leqslant b$, (3) $k - l \leqslant N_A - 1 - b$ and (4) $l \geqslant 0$. Incorporating these constraints and putting the above together, the negativity of a bipartition $B - \bar{B}$ with $\mathrm{card}(B) = b$ is

$$\begin{aligned} \mathcal{N}_{B-\bar{B}} &= -\frac{1}{2}\left\{1 - \sum_{\boldsymbol{k},\pm} \left|\lambda_{\boldsymbol{k}}^{\pm}\right|\right\} \\ &= -\frac{1}{2}\left\{\{1 - \sum_{k=0}^{N_A-1} \sum_{l=\max\{0,k-N_A+1+b\}}^{\min\{k,b\}} \binom{b}{l}\binom{N_A-1-b}{k-l} \right. \\ &\quad \times \left[\left|\frac{1}{2} p^{N_A-1-k}(1-p)^k + \frac{1}{2}(2p-1) p^{N_A-1-k-b+2l}(1-p)^{k+b-2l}\right| \right. \\ &\quad \left.\left. + \left|\frac{1}{2} p^{N_A-1-k}(1-p)^k - \frac{1}{2}(2p-1) p^{N_A-1-k-b+2l}(1-p)^{k+b-2l}\right|\right]\right\}. \end{aligned}$$

The term in brackets can be rewritten as $p^{N_A-1-k}(1-p)^k \max\{1, (2p-1)p^{2l-b}(1-p)^{b-2l}\}$. Summing over b, i.e., adding up all bipartitions $B-\bar{B}$ with $\mathrm{card}(B)=b$, and using the appropriate combinatorial weights $\binom{N_A-1}{b}$ we arrive at the final result.

(iv) *N_A-qubit W-state*. Written in the computational basis the W-state has N_A^2 nonzero matrix elements all with the same value $1/N_A$. The nonzero matrix elements correspond, in the operator basis, to terms of the form of $|010\cdots0\rangle\langle000\cdots01|$ with one and only one excitation (i.e, a 1) in each of the components. Since we are considering independent decoherence processes, the decay of the coherence of each element is the square of the single-qubit coherence $|C_{0,1}|^2 := c^2 := |2p-1|^2$. The only matrix elements that change under a partial transposition with respect to a bi-partition $B-\bar{B}$ are those which have an excitation in B on the first component (corresponding to the ket $|\ \rangle$ in the above operator basis), and no excitation on the second component (corresponding to the bra $\langle\ |$), or vice versa. For example,

$$\underbrace{|010}_{B}\cdots0\rangle\underbrace{\langle000}_{B}\cdots01| \longrightarrow \underbrace{|000}_{B}\cdots0\rangle\underbrace{\langle010}_{B}\cdots01|.$$

All basis elements of this type get mapped into an element with no support/range in the original single-excitation basis: $|0\mathrm{exc.}\rangle\langle 2\mathrm{exc}|$. Therefore, the only contribution to negative eigenvalues of the transposed state will come from a sub-matrix of the form:

$$\frac{c^2}{N_A}\left(\begin{array}{c|ccc} 0 & 1 & \overset{Y}{\cdots} & 1 \\ \hline 1 & 0 & \cdots & 0 \\ \vdots_{Y} & \vdots & & \vdots \\ 1 & 0 & \cdots & 0 \end{array}\right) = \frac{c^2}{N_A}\left(\sqrt{Y}\vec{v}_+\vec{v}_+^{\,T} - \sqrt{Y}\vec{v}_-\vec{v}_-^{\,T}\right) \tag{34}$$

where the first column/row corresponds to the zero excitation basis element while the rest are two excitation elements. Furthermore, with $b=\mathrm{card}(B)$, the number of transposed matrix elements is $Y = b(N_A-b)$ (i.e., those that have an excitation within B in the ket and no excitation in the bra). One can immediately see that with the choice $\vec{v}_\pm^{\,T} = 1/\sqrt{2Y}(\pm\sqrt{Y}, 1, \ldots, 1)$ the above equality holds. Since the $\{\vec{v}_\pm\}$ form a basis, this is just the spectral decomposition of the sub-matrix, and the eigenvalues are simply $\pm c^2\sqrt{Y}/N_A$. We thus find that the negativity with respect to this partition is $\mathcal{N}_B = 1/N_A\sqrt{b(N_A-b)}$. The minimum is obtained for the smallest partition $\mathcal{N}_{\min} = \sqrt{(N_A-1)}/N_A$, while the average over all $2^{N_A}-2$ partitions results in (33). □

Under the action of this dephasing map the family of GHZ states remains diagonal in the GHZ-type basis [60, 61]. For such states, we can alternatively use graph theoretic methods to obtain the spectrum of the partial transposed operators with respect to any bipartition analytically [63, 64]. The same is true for all graph states, and we have used the graph theoretic methods to also calculate average negativities of linear cluster states and ring cluster states of up to five qubits analytically. However, as the size of the cluster states increases, so does the number of different bipartitions and their respective complexity. These formulae are too long to present here, so we opted to simply include a cluster state in the numerical simulations represented in figure 14(a).

Several observations follow from the analytic results (32) and (33) for independent environments.

(i) Standard GHZ, $|\Psi\rangle$ and W states remain N_A-party distillable for all times, since $\mathcal{N}_{\min}$ only reaches zero asymptotically as $t\to\infty$. This does not hold for the $|\Psi''\rangle$ GHZ, which has one partition that becomes disentangled at finite t, nor for $|\Psi'\rangle$, for which $\bar{\mathcal{N}}$ vanishes at a finite

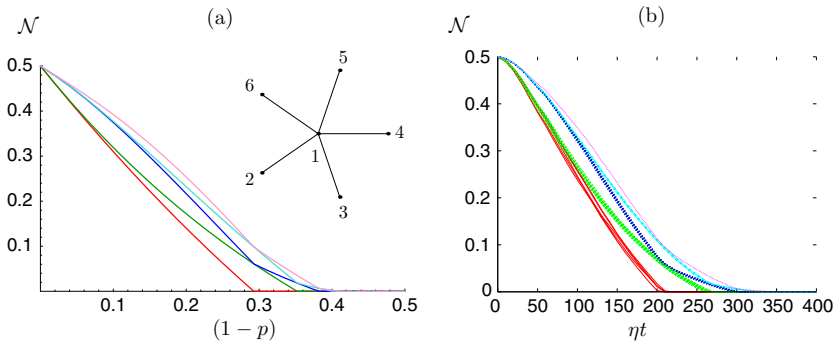

Figure 13. Negativities of all bipartitions in a six-qubit graph GHZ state ($|\Psi'\rangle$). This state can be represented as a star graph (see inset). To name specific partial transpositions we have labelled the qubits (vertices). (a) Analytic curves based on the formula for $|\Psi'\rangle$ in (32). Note that the curves do not cross. We specify the partial transpositions belonging to each curve from top to bottom (where each curve may correspond also to other partial transpositions related to the given one by the symmetries of the star graph): $T_{\{1\}}$, $T_{\{1,2\}}$, $T_{\{1,2,3\}}$, $T_{\{2,3\}}$, $T_{\{2\}}$. (b) Same from a simulation in a lattice gas with 400 spins in a 40×40 lattice (filling factor $\nu = 1/4$) with periodic boundary conditions. The coupling constant is $g_0 = 0.08\eta$. The qubits of the probe particles were placed in the lattice in form of a hexagon with distances as large as possible from each other and did not move themselves. Density matrices were averaged over 100 simulation runs. Although slightly smoothed out, the non-crossing of the negativity curves indicates that the environments of the probe particles were sufficiently independent.

time (all partitions are disentangled; see figure 13). In figure 14(a) we see that $\bar{\mathcal{N}}$ also vanishes at finite time for the cluster state.

(ii) In the limit of large system sizes, the average negativity is, to a very good approximation, given by the negativity of the half-half partition (the distribution of partitions with k particles is sharply peaked at $k = N_A/2$).

(iii) GHZ-type states decay exponentially as we increase the system size N_A, while for W-state the coherences do not vary with the system size, rendering a weak dependence of its average negativity (constant to first order).

(iv) For the states studied here, if a partition is initially more entangled than another, it will remain so also at later times. This does not hold in the presence of correlated collisions, which occur when the distance between probe particles is not large with respect to the relevant times t, i.e., $d < \sqrt{\eta t}$. Figure 13 shows the negativities of all bipartitions of a 6-qubit graph GHZ state (Ψ'). The analytic result demonstrates the statement above, while the simulation shows, that the description with independent environments is good for the parameters used here (see the figure caption).

In finite lattices and after long enough times the above description fails due to inevitable correlated collisions. However, the finite size leads to interesting effects that can also be easily understood. Figure 14(b) shows one such effect: the coherence (and hence the probe's entanglement) lost due to the stochastic interaction with environment spins, is partially recovered after a characteristic revival time. Revivals in a decohering system are usually attributed to a small dimensionality of the environment's Hilbert space. However, in this spin gas, the revival is not due to the finite size of the environment, but to its (effectively) homogeneous coupling to the system[7]. More succinctly, if the lattice is small, all environment

[7] Note that the fact that all environment particle are equally coupled to the probe system, reduces the effective dimension of the environment since only few collective environment states will be coupled.

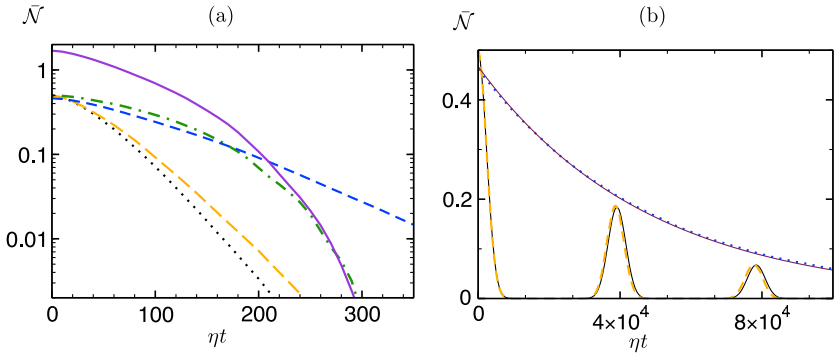

Figure 14. (a) Log-linear plot showing the decay of the average negativity $\bar{\mathcal{N}}$ for six-qubit states: linear cluster state (solid), W-state (short-dashed), and the GHZ states $|\Psi\rangle$ (dotted), $|\Psi'\rangle$ (dash-dotted), and $|\Psi''\rangle$ (long-dashed) in a lattice gas with 400 spins in a 40×40 lattice and coupling constant $g_0 = 0.8\eta$. (b) Entanglement decay of four-qubit GHZ (long-dashed) and W (dotted) states in 20×20 lattice with 25 spins and $g_0 = 8 \times 10^{-3}\eta$ illustrating finite size effects. Single-parameter analytical fits ($\alpha's$) are also shown (thin lines).

particles will have collided approximately the same number of times with the probes after relatively short times, and hence acquired very similar collision phases. Revival will occur when these phases 'simultaneously' reach the value of 2π. So, revival follows rather from the finite size of the lattice, in which the environment particles move, than from the finite number of environment particles. In order to analyse this effect define n_{ak} to be the number of times that particle a of the environment has collided with the probe particle k. At short times, particles neighbouring probe a will collide many times with it before leaving the neighbourhood of a, while far-lying gas particles will need to reach the neighbourhood of a before starting to accumulate nonzero values of n_{ak}. After s time steps a gas particle will typically move distances of the order of $M_s = \sqrt{4\eta(1-\nu)s\delta t}$ sites[8]. After long enough times, all gas particles will have visited every lattice site the same number of times, i.e., $n_{ak} \approx n_{a'k'}$. In this regime we describe the distribution of values n_{ak} by a Gaussian of mean value $\langle n_{ak}\rangle = n = 4s/M^2$ and the variance $\sigma^2 = \langle (n_{ak} - n)^2\rangle = \alpha n$, where α depends on the particular lattice model. Moreover, we expect that at long times most blocking effects between environment particles will be washed out, and therefore assume that different environment particles will have independent collision distributions: $\langle n_{ak} n_{a'k}\rangle = \langle n_{ak}\rangle\langle n_{a'k}\rangle$. Hence, the total effect of N_B on a particular coherence will scale as C^{N_B}, where C is the decay factor of the coherence due to a single environment particle. Taking into account (30) and that the accumulated phase between a probe and a gas atom is given by $\varphi_{ak} = n_{ak}\delta\varphi$ we find that the value of C will in general be given by an average taken over a Gaussian of mean φ_0 and width σ_φ:

$$C = \langle \cos(2\varphi)\rangle = \cos(2\varphi_0)\exp\left(-8\sigma_\varphi^2\right).$$

The phase φ is a sum of the collision phases (with the corresponding signs) involved in the particular coherence: for a coherence specified by binary vector $\boldsymbol{z}_A = \boldsymbol{s}_A - \boldsymbol{s}'_A$, $\varphi = \boldsymbol{z}_A \cdot \boldsymbol{\Gamma}_k = \sum_a (\boldsymbol{z}_A)_a \varphi_{ak}$. For example, for a standard GHZ all phases are added $\varphi = \sum_{a=1}^{N_A} \varphi_{ak}$ leading

[8] After s time steps a gas particle moves a distance $\vec{r} = \sum_{i=1}^{s} \vec{r}_i$ with $\{\vec{r}_i\}_{i=1}^{5} = \{\pm\hat{e}_x, \pm\hat{e}_y, 0\}$, where all unit-displacements occur with equal probability $\eta(1-\nu)\delta t$—the factor $(1-\nu)$ accounts for target positions that are occupied, and hence blocked, by other gas particles. The expected distance will vanish $\langle\vec{r}\rangle = 0$ and the variance will grow as the number of steps: $\langle r^2\rangle = \sum_{ij}\langle\vec{r}_i\cdot\vec{r}_j\rangle = \sum_{ij}\langle\vec{r}_i\cdot\vec{r}_i\rangle\delta_{ij} = \sum_{i=1}^{s} 4\eta(1-\nu)\delta t = 4s\eta(1-\nu)\delta t$.

to a mean value $\varphi_0 \approx N_A n \delta\varphi$ and a variance $\sigma_\varphi^2 \approx \alpha' N_A n \delta\varphi^2$. The factor α' (and α'' below) also includes the contribution of $\langle n_{k'} n_k \rangle - n^2 \propto n$, which depends on the distance between the probe particles k, k'. For the W-state and a given coherence, say $\rho_{w_1 w_2}$, the phase is $\varphi = \varphi_{1k} - \varphi_{2k}$, leading to a vanishing mean value and to a purely exponential decay with $\sigma_\varphi^2 \approx \alpha'' 2 n \delta\varphi^2$, which is independent of the system size N_A. The exponential decay of the W-state and the periodic revival of the GHZ state can be clearly identified in figure 14(b). In this figure we also include the analytic results that follow from the decay of coherences predicted by this simple model and the above expressions for the negativity[9]. The values for the α's used in the model have been fitted to the numerical data.

6. Summary

In this paper we have shown how the class of weighted graph states naturally emerges from graph states by weakening one defining property. Although the weighted graph states can no longer be described in a stabilizer formalism—on which the importance of graph states partly relies—they retain computational accessibility since reduced density matrices of a limited number of particles can be computed efficiently for arbitrarily large systems. To obtain this result we have used techniques based on a projected entangled pairs picture that we have also extended to maps instead of states, suitable for decoherence studies. Alternatively, we have given formulae for the density matrices based on the adjacency matrix of the weighted graph. Both techniques are equivalent and merely reflect a different way of thinking about the possible underlying physical systems. From the reduced density matrices one can compute correlation functions and entanglement measures like the negativity or the von Neumann entropy of entanglement.

Weighted graph states describe spin systems that interact by an Ising-type interaction. We have applied the weighted graph state techniques first to spin chains and lattices, where we have assumed long-range interactions that depend on the distance between spins according to some power law. Using the subadditivity properties of the entropy of entanglement we have derived area laws for the scaling of block-wise entanglement in d-dimensional lattices. In one dimension, we have given a sufficient condition for saturation of entanglement, and we have found that, even in these cases, the correlation length and hence the entanglement length still diverge.

Disordered spin systems with Ising-type interactions are described by random weighted graph states. We have studied the entanglement properties of random weighted graph states and have found that the entropy of entanglement of any subsystem is maximal in the limit of an infinite graph. Spin gases are special disordered spin systems, a prototype of which is the semi-quantal Boltzmann gas. For this gas we have analysed the time-evolution in different temperature regimes and have characterized the equilibrium state and its entanglement properties. In a lattice gas where the correlations due to the geometry of the setup cannot be neglected as in a dilute Boltzmann gas, we have studied numerically the effects of such correlations on the dynamical entanglement properties. Correlated and uncorrelated collision events leave their hallmark on the entanglement time-evolution in such systems.

The whole interaction history of a spin gas is reflected in the weighted graph state that describes it. Hence, such correlated or uncorrelated collision events also lead to non-Markovian or Markovian decoherence processes when the gas acts as a spin bath on some system. We have studied these effects, in particular the robustness of multipartite states, and

[9] Where the scaling of coherences obtained from uncorrelated channels must be replaced by the corresponding correlated ones given by the model (C^{N_B} above).

also finite size effects such as the spontaneous revival of system entanglement previously lost to the spin bath.

Acknowledgments

This work was supported by the Austrian Science Foundation (FWF) and the European Union (OLAQUI, SCALA, QICS). WD acknowledges support from the ÖAW through project APART, JC from the Spanish MCyT under Ramón y Cajal, FIS2005-01369 and Consolider-Ingenio 2010, project QOIT, and CIRIT SGR-00185.

References

[1] Vidal G 2003 *Phys. Rev. Lett.* **91** 147902
[2] Hillery M, Bužek V and Berthiaume A 1999 *Phys. Rev.* A **59** 1829–34
[3] Chen K and Lo H K 2004 *Preprint* quant-ph/0404133
[4] Dür W, Calsamiglia J and Briegel H J 2005 *Phys. Rev.* A **71** 042336
[5] Hein M, Dür W, Eisert J, Raußendorf R, van den Nest M and Briegel H J 2006 Quantum computers, algorithms and chaos *International School of Physics Enrico Fermi* vol 162 ed G Casati, D Shepelyansky, P Zoller and G Benenti (Amsterdam: IOS) (*Preprint* quant-ph/0602096)
[6] van den Nest M, Miyake A, Dur W and Briegel H J 2006 *Phys. Rev. Lett.* **97** 150504
[7] Dür W, Hartmann L, Hein M, Lewenstein M and Briegel H J 2005 *Phys. Rev. Lett.* **94** 097203
[8] Calsamiglia J, Hartmann L, Dür W and Briegel H J 2005 *Phys. Rev. Lett.* **95** 180502
[9] Hartmann L, Calsamiglia J, Dür W and Briegel H J 2005 *Phys. Rev.* A **72** 052107
[10] Verstraete F and Cirac J I 2004 *Preprint* cond-mat/0407066
[11] Anders S, Plenio M B, Dür W, Verstraete F and Briegel H J 2006 *Phys. Rev. Lett.* **97** 107206
[12] Anders S, Briegel H J and Dür W 2006 in preparation
[13] Diestel R 2005 *Graph Theory* 3rd edn (Heidelberg: Springer)
[14] West D B 2001 *Introduction to Graph Theory* 2nd edn (Upper Saddle River, NJ: Prentice-Hall)
[15] Raussendorf R, Browne D E and Briegel H J 2003 *Phys. Rev.* A **68** 022312
[16] Briegel H J and Raussendorf R 2001 *Phys. Rev. Lett.* **86** 910–3
[17] Calderbank A R and Shor P W 1996 *Phys. Rev.* A **54** 1098–1105
[18] Steane A M 1996 *Phys. Rev. Lett.* **77** 793–7
[19] Gottesmann D 1997 *PhD Thesis* California Institute of Technology, Pasadena
[20] Hostens E, Dehaene J and Moor B D 2005 *Phys. Rev.* A **71** 042315
[21] Hein M 2005 *PhD Thesis* University of Innsbruck
[22] Verstraete F and Cirac J I 2004 *Phys. Rev.* A **70** 060302
[23] Cirac J I and Zoller P 2000 *Nature* **404** 579–81
[24] Horn R A and Johnson C R 1991 *Topics in Matrix Analysis* (Cambridge: Cambridge University Press)
[25] Nielsen M A and Vidal G 2001 *Quantum Inf. Comput.* **1** 76–93
[26] Meyer D A and Wallach N R 2002 *J. Math. Phys.* **43** 4273–8
[27] Brennen G K 2003 *Quantum Inf. Comput.* **3** 619–26
[28] Aschauer H, Calsamiglia J, Hein M and Briegel H J 2004 *Quantum Inf. Comput.* **4** 383–95
[29] Verstraete F, Popp M and Cirac J I 2004 *Phys. Rev. Lett.* **92** 027901
[30] Laustsen T, Verstraete F and van Enk S J 2003 *Quantum Inf. Comput.* **3** 64–83
[31] Werner R F and Wolf M M 2001 *Phys. Rev.* A **64** 032112
[32] Zukowski M and Brukner C 2002 *Phys. Rev. Lett.* **88** 210401
[33] Eisert J and Briegel H J 2001 *Phys. Rev.* A **64** 022306
[34] Brennen G K, Caves C M, Jessen P S and Deutsch I H 1999 *Phys. Rev. Lett.* **82** 1060–3
[35] Jané E, Vidal G, Dür W, Zoller P and Cirac J I 2003 *Quantum Inf. Comput.* **3** 15–37
[36] Hein M, Eisert J and Briegel H J 2004 *Phys. Rev.* A **69** 062311
[37] Arnesen M C, Bose S and Vedral V 2001 *Phys. Rev. Lett.* **87** 017901
[38] Osborne T J and Nielsen M A 2002 *Phys. Rev.* A **66** 032110
[39] Osterloh A, Amico L, Falci G and Fazio R 2005 *Nature* **416** 608–10
[40] Vidal G, Latorre J I, Rico E and Kitaev A 2003 *Phys. Rev. Lett.* **90** 227902
[41] Latorre J I, Rico E and Vidal G 2004 *Quantum Inf. Comput.* **4** 48
[42] Damski B, Zakrzewski J, Santos L, Zoller P and Lewenstein M 2003 *Phys. Rev. Lett.* **91** 080403

[43] Sen De A, Sen U, Ahufinger V, Briegel H J, Sanpera A and Lewenstein M 2005 *Preprint* quant-ph/0507172
[44] Page D N 1993 *Phys. Rev. Lett.* **71** 1291–4
[45] Hayden P, Leung D W and Winter A 2006 *Commun. Math. Phys.* **265** 95–117
[46] Greiner M, Mandel O, Esslinger T, Hänsch T W and Bloch I 2002 *Nature* **415** 39–44
[47] Mandel O, Greiner M, Widera A, Rom T, Hänsch T W and Bloch I 2003 *Nature* **425** 937–40
[48] Paredes B, Widera A, Murg V, Mandel O, Fölling S, Cirac I, Shlyapnikov G V, Hänsch T W and Bloch I 2004 *Nature* **429** 277–81
[49] Jaksch D, Bruder C, Cirac J I, Gardiner C W and Zoller P 1998 *Phys. Rev. Lett.* **81** 3108–11
[50] Hofstetter W, Cirac J I, Zoller P, Demler E and Lukin M D 2002 *Phys. Rev. Lett.* **89** 220407
[51] Duan L M, Demler E and Lukin M D 2003 *Phys. Rev. Lett.* **91** 090402
[52] Micheli A, Brennen G K and Zoller P 2006 *Nature Phys.* **2** 341
[53] Lewenstein M, Sanpera A, Ahufinger V, Damski B, Sen De A and Sen U 2006 *Preprint* cond-mat/0606771
[54] Widera A, Gerbier F, Folling S, Gericke T, Mandel O and Bloch I 2005 *Phys. Rev. Lett.* **95** 190405
[55] Zurek W H 2003 *Rev. Mod. Phys.* **75** 715
[56] Leggett A J, Chakravarty S, Dorsey A T, Fisher M P A, Garg A and Zwerger W 1987 *Rev. Mod. Phys.* **59** 1–85
[57] Prokof'ev N V and Stamp P C E 2000 *Rep. Prog. Phys.* **63** 669–726
[58] Wootters W K 1998 *Phys. Rev. Lett.* **80** 2245–8
[59] Vidal G and Werner R F 2002 *Phys. Rev.* A **65** 032314
[60] Dür W and Cirac J I 2000 *Phys. Rev.* A **61** 042314
[61] Dür W and Cirac J I 2000 *Phys. Rev.* A **62** 022302
[62] Eisert J 2001 *PhD Thesis* University of Potsdam
[63] Hein M, Dür W and Briegel H J 2005 *Phys. Rev.* A **71** 032350
[64] Dür W and Briegel H J 2004 *Phys. Rev. Lett.* **92** 180403